FISSION IN EXOTIC NUCLEI USING DENSITY FUNCTIONAL THEORY

By

Zachary Matheson

A DISSERTATION

Submitted to
Michigan State University
in partial fulfillment of the requirements
for the degree of

Physics — Doctor of Philosophy
Computational Mathematics, Science and Engineering — Dual Major

2019

ABSTRACT

FISSION IN EXOTIC NUCLEI USING DENSITY FUNCTIONAL THEORY

By

Zachary Matheson

This is my abstract.

Dedicated to I dunno

ACKNOWLEDGMENTS

I dunno who to acknowledge, either

TABLE OF CONTENTS

LIST OF FIGURES . . . . . **vii**

Chapter 1 Introduction **1**
1.1 History of Fission Theory 1
1.1.1 Liquid Drop Model 2
1.1.2 Strutinsky shell correction 2
1.1.3 Self-consistent models and the supercomputing era 3
1.2 Predicting fission fragments 4
1.3 Goals of the project 5

Chapter 2 Describing Fission Using Nuclear Density Functional Theory **7**
2.1 Nuclear Density Functional Theory 8
2.1.1 Density Functional Theory 9
2.1.1.1 Kinetic term 11
2.1.1.2 Coulomb interaction 12
2.1.1.3 Skyrme interaction 12
2.1.1.4 Pairing interaction 13
2.1.2 Bogoliubov transformation 13
2.1.3 Hartree-Fock-Bogoliubov Equations 14
2.1.4 Nucleon localization function 16
2.2 Microscopic Description of Nuclear Fission 16
2.2.1 Potential Energy Surfaces 17
2.2.2 Collective inertia 17
2.2.3 WKB Approximation 18
2.2.4 Langevin Dynamics 19

Chapter 3 Two fission modes in ^{178}Pt **21**
3.1 Asymmetric fission in the region of ^{180}Hg 21
3.2 Multimode fission of ^{178}Pt 23
3.3 The physical origin of fragment asymmetry in the region of ^{180}Hg 25

Chapter 4 Cluster decay in ^{294}Og **28**
4.1 Cluster emission in Superheavy Elements 28
4.2 Predicted spontaneous fission yields of ^{294}Og 30
4.3 Fragment formation in ^{294}Og 36
4.4 Experimental efforts to find cluster emission in ^{294}Og 36

Chapter 5 Fission in the r-process **40**
5.1 The role of fission in the astrophysical r-process 40
5.2 Fission fragment yields for r-process nuclei 43
5.3 ^{254}Cf 44

Chapter 6 Outlook **46**
6.1 Review, outlook, and perspectives 46

APPENDICES **49**
Appendix A Fragment Identification 50
A.1 Fragments and the Nucleon Localization Function 50
A.2 The problem of scission 51
A.3 Prefragment shell structure 52
A.4 Isospin transport 53
Appendix B Temperature-Dependent ATDHFB Collective Inertia 55
B.1 55

LIST OF FIGURES

Figure 3.1: Survey of fragment yields near ^{180}Hg 23

Figure 3.2: ^{178}Pt experimental data 24

Figure 3.3: UNEDF1-HFB potential energy surface for ^{178}Pt 25

Figure 3.4: D1S potential energy surface for ^{178}Pt 26

Figure 4.1: Calculated and experimental decay modes for SHE 29

Figure 4.2: Dominant decay modes for SHE in a nuclear DFT-based framework. . . 29

Figure 4.3: PES comparison for ^{294}Og using EDFs UNEDF1$_{\mathrm{HFB}}$, D1S, and SkM*. . 32

Figure 4.4: N-Z fission fragment yields from ^{294}Og 34

Figure 4.5: ^{294}Og heavy fragment masses and charges. 35

Figure 4.6: Nucleon localization visualization of ^{294}Og prefragment formation. . . . 37

Figure 5.1: Schematic overview of the r-process 41

Figure 5.2: Final r-process abundances for a neutron star merger scenario with different fission fragment distributions. 42

Figure 5.3: Isotopes whose fission yields are especially relevant to the r-process . . . 43

Chapter 1

Introduction

1.1 History of Fission Theory

Nuclear fission is the fundamental physical process by which a heavy nucleus decays to two smaller nuclei with approximately equal masses, and a proper understanding of fission is critical for applications in reactor physics, nuclear astrophysics, and stockpile stewardship. Fission was first observed by Hahn and Straßmann in 1939 [1] as they bombarded uranium atoms with neutrons and detected barium, but at the time the men could not explain their observations. The explanation came shortly thereafter in a brief letter to the editor by Meitner and Frisch [2], in which they said "On account of their close packing and strong energy exchange, the particles in a heavy nucleus would be expected to move in a collective way which has some resemblance to the movement of a liquid drop. If the movement is made sufficiently violent by adding energy, such a drop may divide itself into two smaller drops…It seems therefore possible that the uranium nucleus has only small stability of form, and may, after neutron capture, divide itself into two nuclei of roughly equal size (the precise ratio of sizes depending on finer structural features and perhaps partly on chance).". A different form of fission, dubbed spontaneous fission because it occurred without bombardment by neutrons or any other projectiles, was reported by Flerov and Petrjak in a single-paragraph letter to *Physical Review* in 1940 [3]. For the remainder of this dissertation, I will be referring

mainly to spontaneous fission unless stated otherwise.

Fission is easy to understand qualitatively but remarkably difficult to explain quantitatively. Theoretically, making predictions about fission is challenging because, thanks to the large number of particles involved and the complex collective interactions which take place when one system deforms and becomes two, fission calculations have an "inextinguishable thirst for computing power," as stated in [4]. One could argue that nuclear fission theory has leapt forward in three major waves.

1.1.1 Liquid Drop Model

The first major wave of nuclear fission theory goes back to the very beginning of the nuclear age, with the liquid drop model in the 1930s. The liquid drop model was developed by Weizsäcker in 1935 [5] as a way of describing the collective properties of nuclei. It was later adapted by Bohr and Wheeler to quantitatively describe nuclear fission in terms of bulk properties of nuclei [6]. This model was able to successfully describe nuclear binding energies and the energetics of nuclear fission.

1.1.2 Strutinsky shell correction

The second wave came with Strutinsky's microscopic correction in the late 1960s, which essentially amounted to adding a quantum mechanical correction to the liquid drop energy. This correction, based on the nuclear shell model, is added in order to better account for the added stability that occurs when a nucleus contains a "magic number" of protons and/or neutrons [7–9]. This is necessary, for instance, in order to explain the occurrence of fission fragments of unequal mass. These models go by the name "microscopic-macroscopic" be-

cause they combine the "macroscopic" bulk properties of the liquid-drop model with the "microscopic" quantum mechanical Strutinsky shell corrections.

These microscopic-macroscopic ("micmac") fission models are computationally fairly inexpensive, and can achieve quite satisfactory results. However, since the model is based on a phenomenological description of what is actually a quantum mechanical system, its predictive power is limited, and there is no clear way of making systematic improvements. A more reliable approach would be to consider the individual nucleon states using some kind of quantum many-body method.

1.1.3 Self-consistent models and the supercomputing era

The third major wave is taking place now, heralded by the age of supercomputers. For large systems with many, many particles, density functional theory (DFT) is a way to recast the Schrödinger equation involving $\sim$200 particles into a simpler problem involving only a few densities and currents (see section 2.1.1). With DFT as a way of calculating nuclear properties quantum-mechanically, one can then combine self-consistent methods developed over the past several decades with modern high-performance computing platforms to predict fission properties, such as lifetimes and fragment yields. Fortunately, a great deal of work has been done to achieve exactly this (see the review article [4]). Some of the ideas which are used were inspired by lessons learned from micmac and other, simpler models; others are unique to DFT. Our approach is described in detail in chapter 2.

These advances in computing come simultaneously with advances in accelerator design and technology and other advances which allow experimental nuclear physics to reach far beyond what has been done before. For instance, the Facility for Rare Isotope Beams (FRIB) at Michigan State University is projected to be able to nearly double the number of isotopes

that can be produced synthetically [10]. Together, state-of-the-art facilities for experiment and high-performance computing for theory are expected to lead to rapid advancement in our understanding of atomic nuclei.

1.2 Predicting fission fragments

Microscopic models (as self-consistent models are often called) are increasingly able to predict properties of fission fragments; however, a comprehensive description of fission fragments (including mass and fragment yields, excitation and kinetic energy distributions, angular dependence, spin, neutron emission) in a microscopic framework remains elusive. In Chapter 2 I will discuss two different approaches for describing the characteristics of fission fragments. In either case, the challenge, now, is to do these calculations cheaply. In every theoretical calculation, one must ask oneself "What approximations can I safely make?" and "What are the important degrees of freedom for this problem?" One may also reduce the total time-to-answer via improvements to the computational workflow itself, such as better file handling and parallelization.

A major source of this elusiveness is due to the sheer difficulty of describing a smooth transition from one nucleus to two, a concept which is plagued with ambiguities. How can one precisely identify two distinct fragments when the wavefunctions of one fragment's constituent nucleons may extend into the opposite fragment? And how do those correlations between nucleons affect the energetics of the resulting fragments? We will briefly address these questions as well in Chapter A.

1.3 Goals of the project

By far the most commonly-studied region so far for fission has been the region of actinides near ^{235}U, which includes isotopes of uranium, plutonium, and thorium relevant for nuclear energy/reactor physics and stockpile stewardship/defense. Isotopes in this region tend to fission asymmetrically, with the larger prefragment influenced by the shell structure of ^{132}Sn and resulting in a heavy fragment distribution centered around $\sim^{140}$Te. However, recent experiments have highlighted other forms of fission which take place in other regions of the nuclear chart.

Given the aforementioned recent interest in rare and exotic nuclei, we have applied our model to study spontaneous fission in exotic systems found in other regions of the nuclear chart, with a focus on primary fragment yields. First, in chapter 3 we discuss bimodal fission in the neutron-deficient isotope platinum-178, which until recently was expected to fission symmetrically. This region is a good one in which to test fission models because of the large isospin asymmetry ($N/Z \approx 1.3$, compared to $N/Z \approx 1.5$ near the valley of stability) Then in chapter 4 we discuss cluster radioactivity in oganesson-294, the heaviest element ever produced by humans. In chapter 5 we move to the neutron-rich side of the nuclear chart ($N/Z > 1.8$ for 290Fm but not $^{254}_{98}\mathrm{Cf}_{156}$) to study isotopes which are expected to play a major role in the astrophysical r-process. **Along the way, we will discuss some of the issues related to fragment identification and yield prediction.**

The calculations in chapters 3, 4, and 5 are relatively expensive. To perform large-scale exploratory studies in other regions of the nuclear chart, it will be necessary to find ways to reduce the total computational cost of these calculations. One method, still in its infancy, offers a promising approach for identifying fission fragment distributions using a

significantly-reduced potential energy surface, which is by far the biggest bottleneck in our calculations. In chapter A, we discuss the problem of scission and present an alternative method for identifying fragments based on the nucleon localization function.

Alternatively, at the end of each chapter, we say a few words about challenges faced during the project and new physical insights gained that aren't related to the overall narrative of the chapter, but which are nevertheless useful for future model developments.

Finally, in chapter 6 we discuss the current state of the field, and, based on our experience, offer insights for guiding future developments in the field.

Chapter 2

Describing Fission Using Nuclear Density Functional Theory

Today there are 2 microscopic approaches to spontaneous fission that are in common use: time-dependent and static (time-independent). Time-dependent approaches evolve the system in real-time. Since fission is an inherently time-dependent process, these methods offer great insight into the fission process and the characteristics of the fragments, especially kinetic and excitation energies [11–15]. However, they can only treat a single event at a time and are quite expensive, making them impractical for fission yield predictions. Despite efforts such as [16, 17], there is currently no way to obtain a full yield distribution in a time-dependent framework. Furthermore, time-dependent computations tend to break down after too many time steps, making them unsuitable for tunneling. This is a problem because spontaneous fission is fundamentally a quantum mechanical tunneling process.

On the other hand, static approaches assume that collective motions of the nucleus are slow compared to the motion of the intrinsic particles, and therefore that collective and intrinsic degrees of freedom can be decoupled. This assumption, called the adiabatic approximation, justifies the creation of a potential energy surface (PES) in some space of collective shape coordinates. The dynamics of fission are then described as trajectories across the PES. Calculating the kinetic and excitation energies in this framework is straightforward

in principle, but in practice it is extremely sensitive to the scission configurations used. However, the static approach is much better suited to estimating fission yields and half-lives.

As we are trying to be as self-consistent as possible, we compute the PES in the framework of nuclear density functional theory, which combines the Hartree-Fock-Bogoliubov (HFB) mean-field approximation to the energy with a many-body method inspired by Kohn-Sham density functional theory (DFT). An overview of the self-consistent framework is described below, followed by the dynamical calculations which we use to calculate fission properties.

2.1 Nuclear Density Functional Theory

Since nuclei are quantum mechanical systems, they can in principle be described using the Schrodinger equation. However, in practice one finds this type of description difficult or impossible, for two reasons:

- In order to use the Schrodinger equation, one needs to know how to describe the interaction between particles, such as between protons and neutrons. However, protons and neutrons are made up of quarks and gluons, which interact via the strong nuclear force. Consequently, an analytic expression for the nucleon-nucleon interaction analogous to the $\frac{1}{r}$ form of the Coulomb interaction is not available. Finding different mathematical expressions which can describe the interaction between nucleons continues to be an active area of research [**?**]

- Even when an interaction is known, nuclei are large systems made up of many protons and neutrons. Solving the Schrodinger equation directly quickly becomes computationally intractable as the number of nucleons increases.

2.1.1 Density Functional Theory

Kohn-Sham DFT is based on the Hohenberg-Kohn theorems

Let us define the nucleon density in the following way: suppose we have a system described in second quantization by a set of creation and annihilation operators $c_i, c_i^\dagger$ which act on the [Fock-space?] vacuum state $|\psi_0\rangle$. The first Kohn-Sham theorem says that the energy of the system is a uniquely-defined functional of the density. That means that if a system of interacting particles and a system of noninteracting particles give the same density, the energy of those systems will be the same. This gives us the freedom to try to describe our system using a mean-field method instead of having to describe the pairwise interactions between every particle in the system - a huge simplification to the problem!

The second Kohn-Sham theorem states that the functional which gives the energy of the system will give the ground state energy if, and only if, it acts on the true ground state density. Thus, given a particular functional, we can vary the input density to minimize the total energy and be assured that we are approaching the ground state energy of the system.

Suppose you have the density $\rho(\mathbf{r})$ of an interacting system of particles. There exists a unique noninteracting system with the same density Then I believe HFB is put on top of that to do the variation part. I think I (approximately) get it now! - So just to make sure, what would DFT look like without HF/HFB? And HF/HFB without DFT?

Rather than find the density of a system of interacting particles (which can be extremely complicated - as one particle moves, the force it exerts on neighboring particles causes them to move, which will in turn change the magnitude and direction of the net force acting on the original particle, and so on until an equilibrium configuration, if it exists, can be attained), Kohn-Sham allows us to find an equivalent density of fictional non-interacting

particles. That is, instead of particles moving in a field generated by many interdependent neighboring particles, one may think of non-interacting particles moving about a mean-field, which is essentially an averaging over all other particles.

Together, the Hohenberg-Kohn theorems state that if one is able to find the true ground state density, regardless of where it comes from, then there exists a unique functional of the density which gives the ground state energy of the system. However, HK do not specify how this functional is to be obtained.

For a variety of reasons/complications (refs 73-78 of [4]), pure Kohn-Sham is not used in nuclear physics; however; in the spirit, we oftentimes switch to a representation involving densities (which are directly and exactly attainable from a many-body wavefunction) and energy density functionals (which are not known exactly). (Wait, but then what is the point of converting to densities? Why not just leave them as wavefunctions? Or maybe we do, but this representation just makes the math look nicer for papers)

The basic idea is to replace the single particle states $c_i^\dagger |\psi_0\rangle$ with the single-particle density, $\rho_{ij} = \langle\psi_0|c_j^\dagger c_i|\psi_0\rangle$

Because pairing interactions are of great importance to nuclear dynamics, we also construct an additional density $\kappa_{ij} = \langle\psi_0|c_j c_i|\psi_0\rangle$, which can be thought of as a coupling between the vacuum state and a state with two particles (in states i and j). Together with the single-particle density ρ we construct a generalized density

$$\mathcal{R} = \begin{pmatrix} \rho & \kappa \\ -\kappa^* & 1-\rho^* \end{pmatrix} \tag{2.1}$$

In coordinate space, the density matrix ρ and the pair tensor κ take the form

$$\rho(\vec{r},\vec{r}') = \langle\psi_0|c^\dagger_{\vec{r}'}c_{\vec{r}}|\psi_0\rangle \tag{2.2}$$

$$\kappa(\vec{r},\vec{r}') = \langle\psi_0|c_{\vec{r}'}c_{\vec{r}}|\psi_0\rangle \tag{2.3}$$

Recall that in nuclei, there is a ρ_n describing neutrons and a ρ_p for protons.

The total energy is a sum of several contributions:

$$E(\rho,\kappa) = E_{kin} + E_{Coul} + E_{nuc} + E_{pair} \tag{2.4}$$

where E_{kin} is the kinetic energy term, E_{Coul} contains the Coulomb interaction between protons, E_{nuc} is a phenomenological nucleon-nucleon interaction term, and E_{pair} describes the tendency of nucleons to form pairs, which is smeared out in non-interacting mean-field models. Finding a good nucleon-nucleon interaction E_{nuc} (and to a lesser extent, E_{pair}) to be used in calculations is an active topic of research in nuclear theory today (for one recent example, see [18]); two types of interactions which are commonly-used today are the Skyrme and Gogny families of interactions `\cite{???}`. We use primarily Skyrme-type interactions, which are described below.

2.1.1.1 Kinetic term

Defining the kinetic density $\tau_\alpha = \nabla\cdot\nabla'\rho_\alpha(\vec{r},\vec{r}')\big|_{\vec{r}=\vec{r}'}$, the kinetic energy contribution is

$$E_{kin} = \frac{\hbar^2}{2m}\left(1-\frac{1}{A}\right)\int d^3\vec{r}\left(\tau_n(\vec{r})+\tau_p(\vec{r})\right) \tag{2.5}$$

The $\left(1-\frac{1}{A}\right)$ term is a simple, approximate center-of-mass correction.

2.1.1.2 Coulomb interaction

The Coulomb interaction between protons is divided into a direct term and an exchange term, which is related to the Pauli exclusion principle.

$$E_{Coul} = E_{Coul,dir} + E_{Coul,exch} \tag{2.6}$$

$$E_{Coul,dir} = \frac{e^2}{2} \int d^3\vec{r}_1 d^3\vec{r}_2 \frac{\rho_p(\vec{r}_1)\rho_p(\vec{r}_2)}{|\vec{r}_1 - \vec{r}_2|} \tag{2.7}$$

$$E_{Coul,exch} = \frac{e^2}{2} \int d^3\vec{r}_1 d^3\vec{r}_2 \frac{\rho_p(\vec{r}_2,\vec{r}_1)\rho_p(\vec{r}_1,\vec{r}_2)}{|\vec{r}_1 - \vec{r}_2|} \tag{2.8}$$

Often the exchange term is computed in the Slater approximation \cite{refs 27,28 of HFODD-I}:

$$E_{Coul,exch} \approx -\frac{3e^2}{4}\left(\frac{3}{\pi}\right)^{\frac{1}{3}} \int d^3\vec{r}\rho_p^{\frac{4}{3}}(\vec{r}) \tag{2.9}$$

2.1.1.3 Skyrme interaction

The total Skyrme interaction energy density is a sum of both time-even and time-odd terms:

$$E_{Skyrme} = \int d^3\vec{r} \sum_{t=0,1} \left(\mathcal{H}_t^{even} + \mathcal{H}_t^{odd}\right) \tag{2.10}$$

$$\mathcal{H}_t^{even} = C_t^{\rho}\rho_t^2 + C_t^{\Delta\rho}\rho_t\Delta\rho_t + C_t^{\tau}\rho_t\tau_t + C_t^{J}\mathsf{J}_t^2 + C_t^{\nabla J}\rho_t\nabla\cdot\vec{J}_t \tag{2.11}$$

$$\mathcal{H}_t^{odd} = C_t^{s}\vec{s}_t^2 + C_t^{\Delta s}\vec{s}_t\Delta\vec{s}_t + C_t^{T}\vec{s}_t\cdot\vec{T}_t + C_t^{j}\vec{\mathsf{j}}_t^2 + C_t^{\nabla j}\vec{s}_t\cdot(\nabla\times\vec{j}_t) \tag{2.12}$$

where τ_t is the kinetic energy density; J_t is the spin current density, with vector part given by $\vec{J}_{\kappa,t} = \sum_{\mu\nu}\epsilon_{\mu\nu\kappa}\mathsf{J}_{\mu\nu,t}$; $\vec{s}_t$ is the spin density, $\vec{T}_t$ is the spin kinetic density; and $\vec{j}_t$ is the

momentum density (to see how these are related to ρ, see, e.g., [19]). The index $t = 0(1)$ refers to isoscalar(isovector) energy densities, e.g., $\rho_0 = \rho_n + \rho_p$ ($\rho_1 = \rho_n - \rho_p$). Note that $\mathcal{H}_t^{even}$ depends only on time-even densities (and likewise for $\mathcal{H}_t^{odd}$).

Since this interaction is phenomenological, based on a zero-range contact interaction between nucleons, the coefficients are adjustable. There are dozens of Skyrme parameterizations on the market, each one optimized to a particular observable or set of observables. The parameter sets SkM* [20] and UNEDF1 [21] (along with its sister, UNEDF1$_{\mathrm{HFB}}$ [22]) are optimized to datasets which include deformed nuclei, making them suitable for fission.

2.1.1.4 Pairing interaction

We use a density-dependent pairing interaction:

$$E_{pair} = V_0 \int d^3\vec{r} \left(1 - \left(\frac{\rho(\vec{r})}{\rho_0}\right)^{\alpha}\right) \tag{2.13}$$

As with the nuclear interaction term, the pairing interaction contains several adjustable parameters.

2.1.2 Bogoliubov transformation

In anticipation of the HFB formalism below, we define the so-called Bogoliubov transformation. The fundamental entity in the Bogoliubov transformed basis are 'quasiparticle' states, defined by quasiparticle creation and annihilation operators acting on a quasiparticle vacuum state $|\Phi_0\rangle$ (in contrast to the single particle operators from before). The creation and annihilation operators are given by

$$\beta_\mu = \sum_i U^*_{i\mu} c_i + \sum_i V^*_{i\mu} c^\dagger_i \tag{2.14}$$

$$\beta^\dagger_\mu = \sum_i U_{i\mu} c^\dagger_i + \sum_i V_{i\mu} c_i \tag{2.15}$$

or in block matrix notation,

$$\begin{pmatrix} \beta \\ \beta^\dagger \end{pmatrix} = \begin{pmatrix} U^\dagger & V^\dagger \\ V^T & U^T \end{pmatrix} \begin{pmatrix} c \\ c^\dagger \end{pmatrix} \equiv \mathcal{W}^\dagger \begin{pmatrix} c \\ c^\dagger \end{pmatrix} \tag{2.16}$$

where the transformation matrix $\mathcal{W}$ must be unitary to ensure that $\beta, \beta^\dagger$ obey the fermion commutation relations [23]. In this transformed basis, the density matrix takes the form

$$\mathsf{R} = \mathcal{W}^\dagger \mathcal{R} \mathcal{W} = \begin{pmatrix} \langle\Phi_0|\beta^\dagger_\mu \beta_\nu|\Phi_0\rangle & \langle\Phi_0|\beta_\mu \beta_\nu|\Phi_0\rangle \\ \langle\Phi_0|\beta^\dagger_\mu \beta^\dagger_\nu|\Phi_0\rangle & \langle\Phi_0|\beta_\mu \beta^\dagger_\nu|\Phi_0\rangle \end{pmatrix} = \begin{pmatrix} 0 & 0 \\ 0 & I_N \end{pmatrix} \tag{2.17}$$

2.1.3 Hartree-Fock-Bogoliubov Equations

The ground state configuration of the system described by this particular energy density functional E is described by the density which minimizes $E(\mathcal{R})$. We can find this solution through the variational principle. We minimize the energy with respect to the generalized density, subject to the constraint that $\mathcal{R}^2 = \mathcal{R}$, or in other words, that the state remains a quasiparticle vacuum. Defining the HFB Hamiltonian $\mathcal{H}_{ba} \equiv 2\partial E/\partial \mathcal{R}_{ab}$, this variation leads to the result $[\mathcal{H}, \mathcal{R}] = 0$, which is called the Hartree-Fock-Bogoliubov equation. It is not typically solved in this form, but it can be recast into something more useful. Recalling that two Hermitian operators whose commutator is zero can be simultaneously diagonalized,

we choose to diagonalize $\mathcal{H}$ using the same Bogoliubov transformation W which diagonalizes $\mathcal{R}$:

$$W^{\dagger}\mathcal{H}W \equiv \mathcal{E} \qquad \text{or} \qquad \mathcal{H}W = W\mathcal{E} \tag{2.18}$$

where

$$\mathcal{E} = \begin{pmatrix} E_{\mu} & 0 \\ 0 & -E_{\mu} \end{pmatrix} \tag{2.19}$$

is a matrix of quasiparticle energies. In this form, the problem can then be solved iteratively: an initial density ansatz is chosen in order to construct the Hamiltonian density $\mathcal{H}$, after which the eigenvalue problem is solved, leading to new densities (since the densities are related to $\mathcal{W}$), which in turn leads to an updated $\mathcal{H}$. This procedure can be repeated indefinitely, until some predetermined convergence criterion is met.

Very often we will want to minimize the energy with the system subject to a particular constraint. In that case we would replace the Hamiltonian E with the Routhian E' before variation. Typically E' introduces the constraints via the method of Lagrange multipliers. Some common examples might be this simple form of particle number restoration (more sophisticated forms, such as Lipkin-Nogami `\cite{???}`, also exist)

$$E' = E - \lambda_n \left\langle \hat{N}_n \right\rangle - \lambda_p \left\langle \hat{N}_p \right\rangle \tag{2.20}$$

where λ_{α} is determined later by the condition that $\left\langle \hat{N}_{\alpha} \right\rangle = N_{\alpha}$, or shape, where we might constrain a particular multipole moment (or set of multipole moments) to the value $\bar{Q}_{\lambda\mu}$

$$E' = E - \sum_{\lambda\mu} C_{\lambda\mu} \left(\left\langle \hat{Q}_{\lambda\mu} \right\rangle - \bar{Q}_{\lambda\mu} \right)^2 \tag{2.21}$$

2.1.4 Nucleon localization function

One of the tools we will be using quite a bit in this thesis is the nucleon localization function (NLF), introduced in [24]. The NLF is defined using the single particle density in the following way (with q=isospin and σ=spin/signature quantum number):

$$\mathcal{C}_{q\sigma} = \left[1 + \left(\frac{\tau_{q\sigma}\rho_{q\sigma} - \frac{1}{4}|\nabla\rho_{q\sigma}|^2 - \mathbf{j}_{q\sigma}^2}{\rho_{q\sigma}\tau_{q\sigma}^{TF}} \right)^2 \right] \tag{2.22}$$

where $\tau_{q\sigma}^{TF} = \frac{3}{5}(6\pi^2)^{\frac{2}{3}}\rho_{q\sigma}^{\frac{5}{3}}$. A localization value $\mathcal{C} \approx 1$ means that nucleons are well-localized; that is, the probability of finding two nucleons of equal spin and isospin at the same location in space is low. A value of $\mathcal{C} = \frac{1}{2}$ corresponds to a Fermi gas of nucleons, as found in nuclear matter.

The NLF offers greater insight into the underlying shell structure of the system than, for instance, the single particle density. In particular, when applied to fission as in [25], it sometimes enables one to see the formation of well-defined prefragments whose shell structure is responsible for the peak of the fragment distribution.

2.2 Microscopic Description of Nuclear Fission

With the nuclear physics somewhat under control, we now move onto the problem of using it to describe fission. Recently in [26], an approach based on this assumption was used to compute fragment yields from a potential energy surface (PES) that was computed self-

consistently, using the WKB approximation to describe the tunneling and Langevin dynamics to describe post-scission dissipation. The half-life can be computed as in [27].

2.2.1 Potential Energy Surfaces

In the adiabatic approximation, the primary degrees of freedom are nuclear shapes, and therefore the basic ingredient to fission calculations is a potential energy surface (PES). In principle, one could describe any three-dimensional shape using an infinite basis such as the multipole expansion which is often encountered in electrodynamics; however, for practical computations one must used a truncated set of only a few collective coordinates. Thus, an important challenge for researchers is to select the most relevant collective coordinates, ideally while demonstrating that others can be safely neglected. Often one will use the first few lowest-order multipole moments; however, multipole moments may not always be well-suited to describing shapes which occur during fission, especially near scission. One alternative was proposed in [28].

Once the appropriate shape constraints are chosen, the PES is computed as a mesh: one DFT calculation per grid point. The value at each point is the HFB energy computed above, $E'(\vec{q})$.

2.2.2 Collective inertia

Just as important to the fission dynamics as the energy of the system is the collective inertia, which describes the tendency of the system to resist configuration changes (such as shape changes). The form of the collective inertia we use is the non-perturbative adiabatic time-dependent HFB (ATDHFB) inertia with cranking [29], which takes the form

$$\mathsf{M}_{\mu\nu} = \frac{\hbar^2}{2}\frac{1}{(E_a + E_b)}\left(\frac{\partial \mathcal{R}^{21}_{(0),ab}}{\partial q_\mu}\frac{\partial \mathcal{R}^{12}_{(0),ba}}{\partial q_\nu} + \frac{\partial \mathcal{R}^{12}_{(0),ab}}{\partial q_\mu}\frac{\partial \mathcal{R}^{21}_{(0),ba}}{\partial q_\mu}\right) \tag{2.23}$$

The subscripts and superscripts are explained in the full temperature-dependent derivation of the collective inertia found in Appendix ???, but the important feature to note is that computing the inertia requires differentiating the density matrix with respect to a set of collective coordinates.

A perturbative expression for the ATDHFB inertia also exists, which allows one to estimate the inertia without taking derivatives of the density. It is computationally much faster and easier to implement, but it is less accurate and loses many of the important features of the inertia, as we shall see in Chapter ??? (294Og). Nevertheless, it is commonly-used in calculations and we shall use it later on.

Another common expression for the collective inertia comes from the Generator Coordinate Method (GCM). The GCM inertia also exists in two varieties: perturbative and non-perturbative [30]. Like the ATDHFB inertia, the perturbative GCM inertia is smoothed-out compared to the non-perturbative inertia. Both the perturbative and non-perturbative GCM inertias are found to be smaller in magnitude than their ATDHFB counterparts.

2.2.3 WKB Approximation

Spontaneous nuclear fission is a type of quantum tunneling; consequently, it should be described using quantum mechanics. If the wavefunction corresponding to the fissioning nucleus is assumed to be slowly-varying inside the potential barrier (which is the case under the adiabatic assumption), then the WKB approximation allows us to estimate the tunneling probability through a classically-forbidden region in the PES.

Consider a set of collective coordinates $\mathbf{q} \equiv (q_1, \ldots, q_N)$. The most-probable tunneling path $L(s)|_{s_{\text{in}}}^{s_{\text{out}}}$ in the collective space is found via minimization of the collective action

$$S(L) = \frac{1}{\hbar} \int_{s_{\text{in}}}^{s_{\text{out}}} \sqrt{2\mathcal{M}(s)\,(V(s) - E_0)}ds, \tag{2.24}$$

where s is the curvilinear coordinate along the path L, $\mathcal{M}(s)$ is the collective inertia given by [27]

$$\mathcal{M}(s) = \sum_{\mu\nu} \mathsf{M}_{\mu\nu} \frac{dq_\mu}{ds} \frac{dq_\nu}{ds} \tag{2.25}$$

and $V(s)$ is the potential energy along $L(s)$. E_0 stands for the collective ground-state energy. The dynamic programming method [31] is employed to determine the path $L(s)$. The calculation is repeated for different outer turning points, and each of these points is then assigned an exit probability $P(s_{\text{out}}) = [1 + \exp\{(2s)\}]^{-1}$ [32].

The half-life corresponds to the minimum action pathway, and the expression for the half-life is $T_{1/2} = \ln(2)/nP(s_{\text{min}})$. The parameter n is the number of assaults on the fission barrier per unit time and the standard value is $n = 10^{20.38} s^{-1}$.

2.2.4 Langevin Dynamics

Two techniques for predicting fission fragment yields are the Langevin approach used by [26] and the Time-Dependent Generator Coordinate Method (TDGCM) approach used in [28]. I will be using Langevin dynamics, which are described in this section.

After emerging from the classically-forbidden region of the PES, fission trajectories begin from the outer turning line and then evolve along the PES according to the Langevin

equations:

$$\frac{dp_i}{dt} = -\frac{p_j p_k}{2}\frac{\partial}{\partial q_i}\left(\mathcal{M}^{-1}\right)_{jk} - \frac{\partial V}{\partial q_i} - \eta_{ij}\left(\mathcal{M}^{-1}\right)_{jk} p_k + g_{ij}\Gamma_j(t)\,, \tag{2.26}$$

$$\frac{dq_i}{dt} = \left(\mathcal{M}^{-1}\right)_{ij} p_j\,, \tag{2.27}$$

where p_i is the collective momentum conjugate to q_i. The dissipation tensor η_{ij} is related to the random force strength g_{ij} via the fluctuation-dissipation theorem, and $\Gamma_j(t)$ is a Gaussian-distributed, time-dependent stochastic variable.

The fluctuation-dissipation theorem is given by the expression $\sum_k g_{ik}g_{jk} = \eta_{ij}k_B T$. It effectively couples the collective and intrinsic via the system temperature, given by $k_B T = \sqrt{E^*/a}$ where $a = A/10\text{MeV}^{-1}$ parameterizes the level density and the excitation energy $E^* = V(s_{out}) - V(\mathbf{x}) - \frac{1}{2}\sum\left(\mathcal{M}^{-1}\right)_{ij} p_i p_j$.

Dissipation is treated in our work as a parameter, as a self-consistent description of dissipation is not yet known. However, work along this line has been started (maybe?) in refs 291-293 of [33] (see section 4.1.1 for the context). In the meantime, we use the values from [26] (Is this too specific for a thesis? You're not worried about the little numerical details, right? Just the big-picture ideas?)

Chapter 3

Two fission modes in ^{178}Pt

3.1 Asymmetric fission in the region of ^{180}Hg

As mentioned in the introduction, fission is most well-studied in the region of the actinides (Z=90 to Z=103), as many naturally-occurring isotopes in this region are fissile. Within this region, there is a characteristic tendency for fission fragment yields to be asymmetric (that is, one light fragment and one heavy fragment), with the heavy peak centered around $A \approx 140$. This has been understood as a manifestation of nuclear shell structure in the prefragments: doubly-magic ^{132}Sn drives the nucleus towards scission, and once the neck nucleons are divided up between the two fragments, we end up with the heavy fragment A=140 peak. As one moves to the lower-Z actinides, however, this tendency becomes less and less pronounced as yields tend to become more symmetric. Below thorium, it was generally believed until recently (though mostly not tested) that yields would continue to be symmetric as there was no doubly-magic nucleus candidate that could drive the system toward asymmetry as there is with actinides.

However, it was reported in a 2010 study [34] that neutron-deficient ^{180}Tl undergoes beta-delayed fission, leading to intermediate state $^{180}_{80}\mathrm{Hg}_{100}$ which then decays into two fragments of unequal mass. This finding triggered a flurry of theoretical papers hoping to describe this new and unexpected phenomenon (for instance, see `\cite{some papers}`). A follow-up

study using ^{178}Tl [35] further established this as a region of asymmetric fission, and not just a one-time occurrence. Since then, other nuclei in the region have been studied, for instance using Coulex-induced fission reactions and compound nucleus (prompt?) fusion-fission reactions, and the finding is the same.

Nuclei in this region have a number of unique features which make them interesting for study, even aside from the unexpected fragment asymmetry. Predicted fission barrier heights in this region are relatively-low (of the order of 12 MeV), making them suitable for study using low-energy techniques such as β-delayed fission (maybe [36] and the work at ISOLDE at CERN?) or Coulex-induced fission (maybe [37] and the SOFIA (Studies On FIssion with Aladin) experiment/project/campaign). On the other hand, it has been found that compound nuclei formed in this region from particle-induced reactions tend to have high excitation energies, even for beam energies near the Coulomb barrier. This combination makes the region particularly well-suited for studies involving a variety of excitation energies.

Later experiments performed with isotopes in this region at different excitation energies have shown that, unlike the case of actinides where shell structure and fragment asymmetry is "washed out" at high excitation energies, mass asymmetric fragment distributions are a persistent feature of this mass region for various excitation energies. (A lot of good citations for this section can come from section 4.1.1 of [38]) An up-to-date (as of around 2016) overview of nuclei in the region of $^{180}_{80}\mathrm{Hg}_{100}$ which have since been experimentally studied, including the experimental technique used, is shown in Figure 3.1.

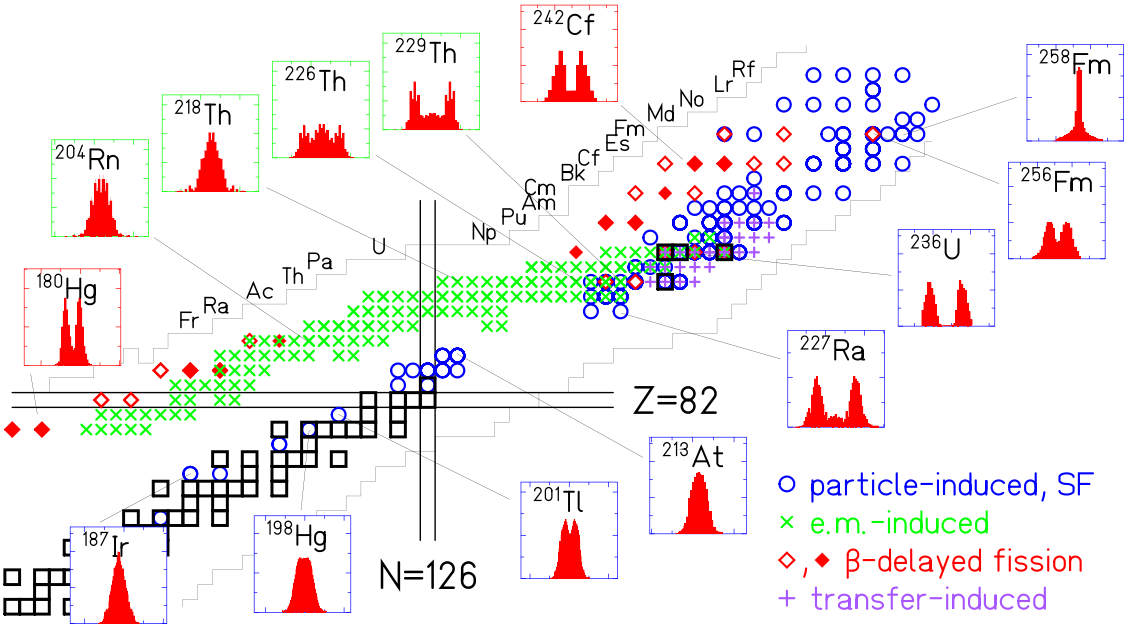

Figure 3.1: Fragment yields for several nuclei ranging from actinides, where primary fission yields tend to be asymmetric, down to near-thorium, where yields become more symmetric except in the region near neutron deficient $^{180}_{80}\mathrm{Hg}_{100}$. Figure from [38].

3.2 Multimode fission of ^{178}Pt

One particular follow-up experiment was performed investigating spontaneous fission of $^{178}_{78}\mathrm{Pt}_{100}$ [**?**], which differs from $^{180}_{80}\mathrm{Hg}_{100}$ by 2 protons. This system was studied at various excitation energies and found to fission consistently with a bimodal pattern, as shown in Figure 3.2. Of the nuclei which underwent spontaneous fission, roughly 1/3 were found to fission symmetrically while the other 2/3 fissioned asymmetrically with a light-to-heavy mass ratio of approximately 79/99. Furthermore, it was observed that symmetric fragments tended to have higher kinetic energies than non-symmetric fragments.

To better interpret the results of this experiment, DFT calculations were performed using the functionals UNEDF1$_{\mathrm{HFB}}$ [22] and D1S [39]. These calculations involved computing a PES using the collective coordinates Q_{20} and Q_{30}. [Do I need to describe the calculations in detail here, or should I refer to the published papers (e.g. "Details of the calculation are

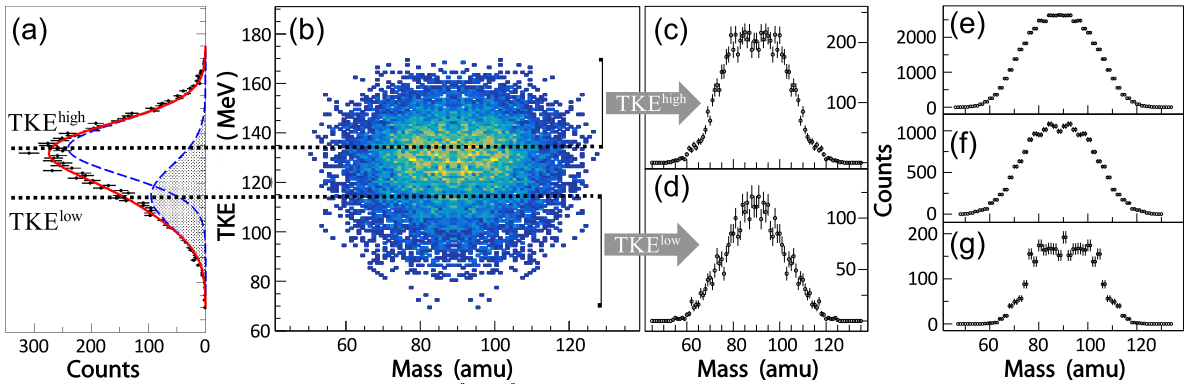

Figure 3.2: This figure contains the data from the $^{178}_{78}\mathrm{Pt}_{100}$ experiment. I should go through and describe what all the individual boxes are for. Then I should cite out paper, once it's citeable

given in `the paper`")?]

The UNEDF1$_{\mathrm{HFB}}$ PES is shown in Figure 3.3, while the D1S PES is in Figure 3.4. A calculation with full Langevin dynamics was not performed; however, the static (minimum-energy) pathway shown in the figure corresponds to a fragment split $A_L/A_H \approx 80/98$.

Also shown in Figure 3.3 are nucleon localization functions (recall Section) corresponding to various configurations in the PES. Along the symmetric path (ABcd in the figure), the fragments appear highly-elongated, with a rather large neck, even shortly before scission. Since elongation tends to minimize the Coulomb repulsion between fragments, then this configuration might be expected to lead to fragments with relatively low kinetic energies. On the other hand, compact fragments such as those in ABCD will tend to have a larger Coulomb repulsion, propelling the fragments away from one another with greater force and resulting in fragments with a higher kinetic energy. [We note that this is compatible with experiment]

Now consider the PES corresponding to the D1S functional in Figure 3.4. We note with some relief that, despite the inherent differences between the functionals, and despite the relative flatness of the surface with few discernible topological features, the overall topology

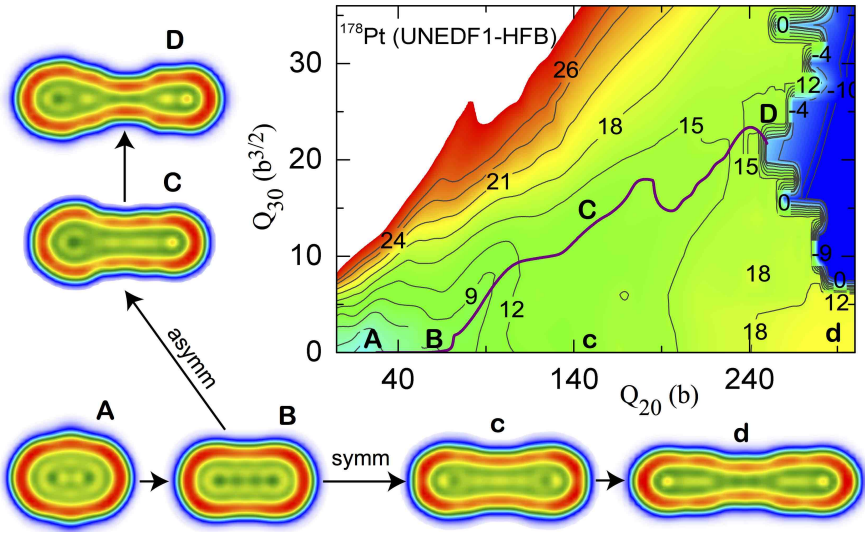

Figure 3.3: UNEDF1-HFB potential energy surface for ^{178}Pt. Note the two different trajectories ABCD and ABcd and their corresponding localizations.

of the PES is similar in both cases. The overall magnitude is different, but the static pathway follows a similar trajectory.

3.3 The physical origin of fragment asymmetry in the region of ^{180}Hg

Why is there a region of symmetric fission below thorium?

(These are notes from the 178Pt paper draft. Not mine, of course, but they have some good points to address): "Namely, the PES are predicetd to be flat and much less structureless, and defined predominantly by the large liquid drop/macroscopic contribution, rather than by relatively small microscopic effects. Due to this, FFMDs exhibit fairly low dependence.. [refer to 180Hg PLB, as one example].

"(this was an answer by Witek, when somebody asked a question to my talk at Tsukuba - why the lead region is less sensitive to temperature.. the answer was - there is no 'barrier'

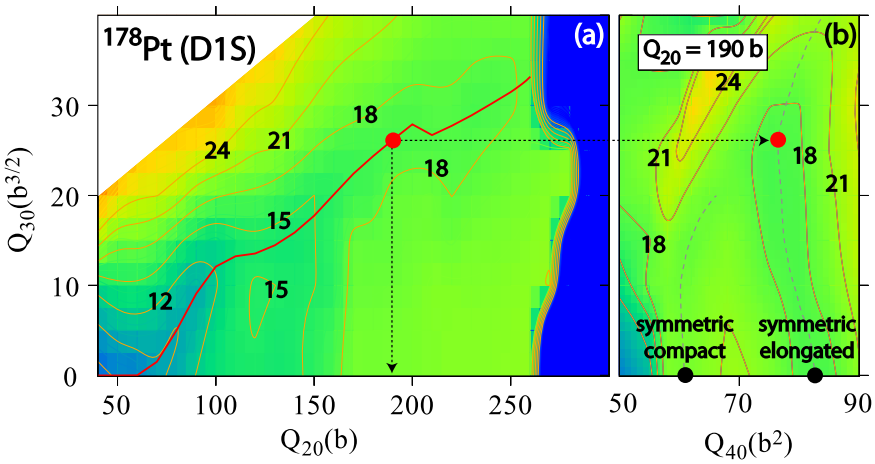

Figure 3.4: D1S potential energy surface for ^{178}Pt. Note also the additional information about the hexadecapole moment.

in a sence, it's just flat/thick macroscopic surface, hardly influenced by shell effects.. so, even if one heats it up, tiny shell effects will be gone, but the main underlying macroscopic part will remain)."

Peter Moller argues in the concluding discussion of (https://link.aps.org/doi/10.1103/PhysRevC.85.024 [40]) that we can't really use the fragment/prefragment shell structure arguments in this region, and thus that we have yet to identify all the essential physics which determines fragments. He says the yields are given (at least in this case) by subtle interplays in local regions of the potential energy surface.

Witek, Michal Warda, and Staszczak argue in Section IV. *Prescission Configurations* of [41] that 180Hg deforms as a molecular system consisting of 90Zr and 72Ge, with the remaining neck nucleons being distributed at scission to give the fragments they found in the experiment. Similarly, they make the same claim for 198Hg, except using 98Zr and 80Ge. The first one kind of makes sense to me since 90Zr is semi-magic, but 98Zr is not and neither is 80Ge. I wonder what might have happened had they tried to match up the densities of a different set of nearby nuclei (they used these because they had the same N/Z ratio as the

fissioning parent nucleus). Then in the conclusions: "We conclude that the mass distribution of fission fragments in both nuclei is governed by shell structure of prescission configurations associated with molecular structures."

In the introduction to [42] it is stated as though conclusively that "the main factor determining the mass split in fission are shell effects at pre-scission configurations, i.e., between saddle and scission" (see also some additional references therein). I think the thing that is most selling it to me so far, though, is Fig. 3 from this paper, wherein they show the shell correction energy for each of the nuclei considered. Even though the PES itself is mostly flat in each of these cases, the magnitude of the shell correction is different whether you are looking at symmetric or asymmetric trajectories, and the one with the larger magnitude shell correction happens to be the one that wins out in the final fragment distribution. I'd also be curious to see what the collective inertia looks like, but this seems to at least give something. It's not like this shell correction gets added on top of the PES - the PES is still relatively-flat - but it at least gives an explanation for why our traditional physical intuition is not totally failing us here.

Interesting future work in this region might include calculations with full dynamics (including from nuclei with excitation energy), as suggested in the conclusions of [42]

Chapter 4

Cluster decay in ^{294}Og

4.1 Cluster emission in Superheavy Elements

The region of superheavy elements (Z>104) is an interesting one for the study of spontaneous fission because the liquid drop model predicts that all isotopes with Z>104 are unstable with respect to spontaneous fission. These nuclei are stabilized due to shell effects, but they nevertheless remain short-lived and many of them will decay by spontaneous fission regardless.

Experimentally, spontaneous fission has been observed from several superheavy isotopes (see the right panel of Figure 4.1). Other observed SHEs undergo a series of alpha decays, which chains terminate in spontaneous fission. Furthermore, a variety of models predict regions of spontaneous fission in the superheavy regime. One example is shown in Figure 4.1, in which lifetimes were computed for several types of decays using empirical formulas and the results compared to estimate branching ratios. Figure 4.2 is similar, except that the spontaneous fission lifetimes were computed microscopically, as were the Q_α values used to estimate alpha decay lifetimes.

cluster emission [45–47]

From the theoretical point of view, half-life calculations based on semiempirical models predict cluster radioactivity to be the dominant decay channel of several superheavy nu-

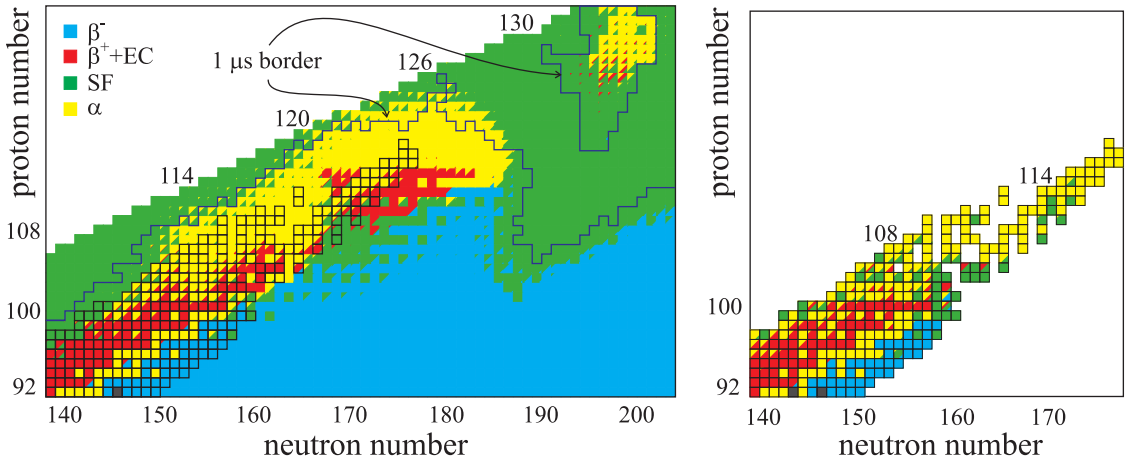

Figure 4.1: Calculated (left) and experimental (right) decay modes for SHE, based on an analysis of lifetimes calculated via empirical formulae. The boxed isotopes in the left panel are those which have been measured experimentally. Isotopes falling inside the 1μs contour are predicted to live longer than 1μs. Figure adapted from [43].

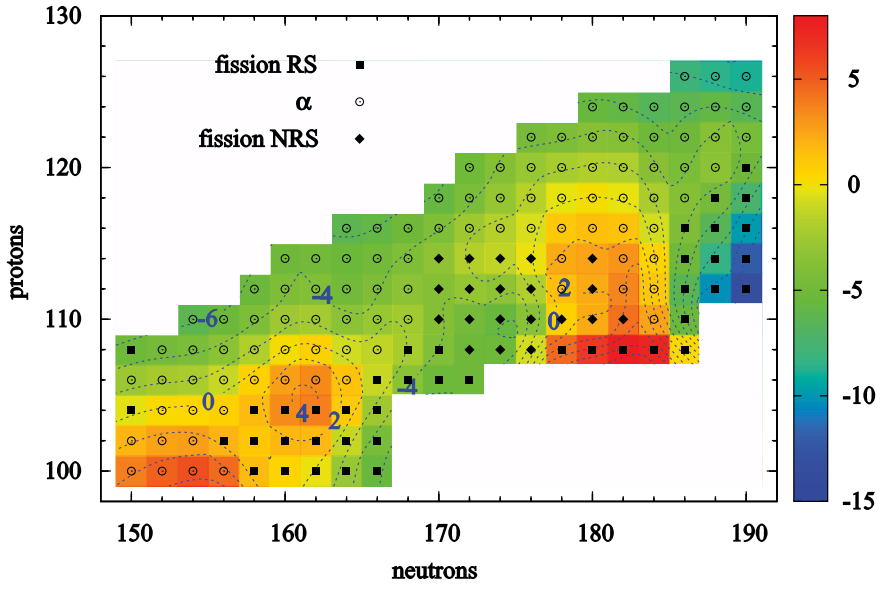

Figure 4.2: Dominant decay modes for SHE in a nuclear DFT-based framework are indicated. The label "RS" stands for "reflection symmetric" and "NRS" stands for "non-reflection symmetric." The colorbar indicates the predicted half-life on a logarithmic scale. Figure from [44].

clei [48–54]. Similar predictions have been obtained by more microscopic calculations using nuclear DFT framework [55, 56].

Poenaru and others have predicted in [48–54] that many superheavy elements will decay into two fragments, with the heavy fragment near the doubly-magic nucleus $^{208}_{82}\mathrm{Pb}_{126}$. This particular decay mode is significant enough to have earned its own name in the literature, where it is known variously as cluster emission, cluster radioactivity, or lead radioactivity [45–47, 57]. The phenomenon of cluster emission was first observed in the decay $^{223}_{88}\mathrm{Ra}\rightarrow^{209}_{82}\mathrm{Pb}$ + $^{14}_{6}$ [58] and has since been observed in several actinides. In all cases seen so far, it is a rare event with a small branching ratio [57].

The mechanism of cluster emission is based on the stability of the doubly-magic nucleus $^{208}_{82}\mathrm{Pb}_{126}$. $^{294}_{118}\mathrm{Og}_{176}$ is an excellent candidate for cluster emission because the cluster it is predicted to emit, $^{86}_{36}\mathrm{Kr}_{50}$, receives additional stability due to its having a magic number of neutrons. Semiemprical arguments based on the symmetry energy lend additional support to this candidate, since $^{294}_{118}\mathrm{Og}_{176}$ and $^{208}_{82}\mathrm{Pb}_{126}$ have a similar N/Z ratio [56].

We took this prediction one step further than the aforementioned by calculating the full spontaneous fission fragment distribution of $^{294}_{118}\mathrm{Og}_{176}$. As we will show, the distribution is sharply-peaked around $^{208}_{82}\mathrm{Pb}_{126}$. Furthermore, the distribution is quite robust with respect to the inputs of the calculations. We will also visualize the formation of the fragments using the nucleon localization function.

4.2 Predicted spontaneous fission yields of ^{294}Og

We calculated the spontaneous fission fragment yields for $^{294}_{118}\mathrm{Og}_{176}$ under a variety of conditions. First, we elected to using three distinct EDFs: UNEDF1$_{\mathrm{HFB}}$[22], a Skyrme functional

which was optimized to data for spherical and deformed nuclei, including fission isomers; SkM* [20], another Skyrme functional designed for fission barriers and surface energy; and D1S [39], a parameterization of the finite-range Gogny interaction fitted on fission barriers of actinides.

A different collective space was used with each EDF for the tunneling portion of the PES. The UNEDF1$_{\mathrm{HFB}}$ calculation was carried out in a four-dimensional collective space consisting of the collective coordinates $(Q_{20}, Q_{30}, Q_{22}, \lambda_2)$. By examining this PES, we were able to reduce to dimensionality of the PES for the other two functionals. The SkM* calculation was performed in a piecewise-continuous space. Between the ground state and the isomer state, Q_{30} does not play a significant role and so the system was described using $(Q_{20}, Q_{22}, \lambda_2)$. Likewise, $Q_{22} \approx 0$ once the isomer state is reached and reflection symmetry is broken ($Q_{30} \neq 0$), suggesting use of the coordinates $(Q_{20}, Q_{30}, \lambda_2)$. Finally, for the functional D1S we decided to see how our yields would be affected if we did not consider dynamical pairing fluctuations or axial symmetry breaking at all, in order to drastically reduce computation time. Those calculations were performed in the collective space (Q_{20}, Q_{30}).

In the region of Langevin dynamics, which is the region connecting the hypersurface of outer turning points and to the hypersurface of scission points, we found again that $Q_{22} \approx 0$. Consequently, this region was limited to two dimensions (Q_{20}, Q_{30}) in all cases.

We start by showing 2-dimensional projections of the calculated PESs in Figure 4.3. Although the collective spaces used are different, it is reassuring to see that the surfaces strongly resemble one another. Some common features we highlight are: a symmetric saddle point occurring around $Q_{20} \approx 40\,\mathrm{b}$; a second barrier beginning around $Q_{20} \approx 100 - 120\,\mathrm{b}$ along the symmetric fission path; the presence of local minima at large deformations (marked by stars in the figure); a deep valley that leads to an highly-asymmetric split; and the

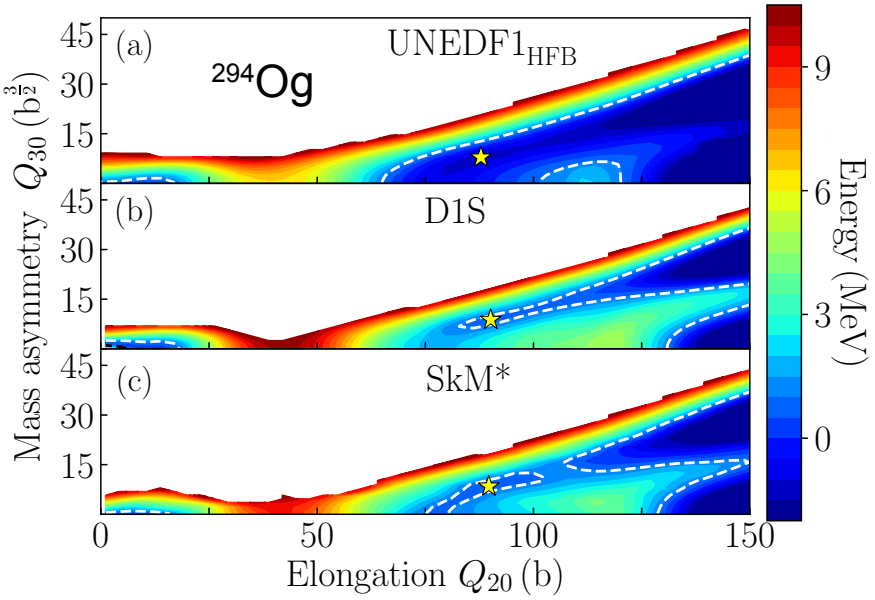

Figure 4.3: Comparison of the PESs for $^{294}_{118}\mathrm{Og}_{176}$ in the (Q_{20}, Q_{30}) collective plane obtained in $\mathrm{UNEDF1_{HFB}}$ (a), D1S (b), and SkM* (c) EDFs. The ground-state energy E_{gs} is normalized to zero. The dotted line in each figure corresponds to $E_0 - E_{gs} = 1\,\mathrm{MeV}$, which was used to determine the inner and outer turning points. The local energy minima at large deformations are marked by stars.

secondary, less-asymmetric fission valley that emerges at large elongations.

But there are differences as well, such as the height of the first saddle point, the depth of the highly-asymmetric fission valley, and the height of the ridge separating the two fission valleys. As a result, the outer turning points are pushed to larger elongations in D1S and SkM* as compared to $\mathrm{UNEDF1_{HFB}}$. These differences in the PES topology strongly affect the predicted spontaneous fission half-lives τ_{SF}, which in the case of $\mathrm{UNEDF1_{HFB}}$, SkM* and D1S are $9.1 \times 10^{-9}\,\mathrm{s}$, $4.0 \times 10^{-5}\,\mathrm{s}$ and $3.2 \times 10^{-2}\,\mathrm{s}$, respectively (see also [59, 60] for a detailed discussion of half-lives). These large variations of τ_{SF} reflect the well-known exponential sensitivity of spontaneous fission half-lives to changes in the quantities entering the collective action (2.24). The τ_{SF} predictions of $\mathrm{UNEDF1_{HFB}}$ and, to a lesser degree, SkM* are incompatible with experiment, as ^{294}Og is known to decay by α-decay with a half-life of 0.58 ms [61]. This observation could in fact also apply to the D1S results, since the

D1S calculations were performed in a smaller collective space leading to overestimation of the half-lives [62, 63]. It is to be noted that while half-lives are very sensitive to details of the calculations, the models used here are very consistent with each other and with experiment when it comes to global observables, such as alpha-decay energies, deformations, and radii [64**?**]. As demonstrated below in Figure 4.4, spontaneous-fission mass and charge yields are also robustly predicted.

As expected, the yields are peaked in the region of ${}^{208}_{82}\mathrm{Pb}_{126}$ with a sharp fall-off. Likewise, the projected distributions onto the mass and charge axes shows a clear preference for cluster emission, as seen in the top panels of Figure 4.5.

As discussed in Chapter 2, the collective inertia can also have a large impact on the fission dynamics. Using the $\mathrm{UNEDF1_{HFB}}$ functional, we compared our result with the non-perturbative cranking ATDHFB inertia $\mathcal{M}^{\mathrm{A}}$ to the perturbative ATDHFB $\mathcal{M}^{\mathrm{AP}}$ (which appears smoothed-out compared to $\mathcal{M}^{\mathrm{A}}$) and perturbative GCM $\mathcal{M}^{\mathrm{GCM}}$ (which is smooth and also lower in magnitude than $\mathcal{M}^{\mathrm{A}}$ or $\mathcal{M}^{\mathrm{AP}}$ by roughly a factor of 1.5), which are often easier to use for large-scale calculations. The result, shown in the middle panels of Figure 4.5, show that the distribution has shifted slightly, but that $\mathcal{M}^{\mathrm{AP}}$ and $\mathcal{M}^{\mathrm{GCM}}$ give identical, or nearly-identical results. The smoothness of the perturbative inertias apparently allow fluctuations to drive the system to more extreme fragment configurations. This suggests that the magnitude of the inertia matters less than the topography for computing fission yields (though we note that this would not be true for calculating half-lives, which depend exponentially on the magnitude of the inertia).

We also vary the strength of fluctuations by adjusting the parameter η. Our starting point η_0 is taken from reference [26], where it was obtained by adjusting η to match the experimental fragment distribution of ${}^{294}\mathrm{Pu}$. Shown in the bottom panel of Figure 4.5, we

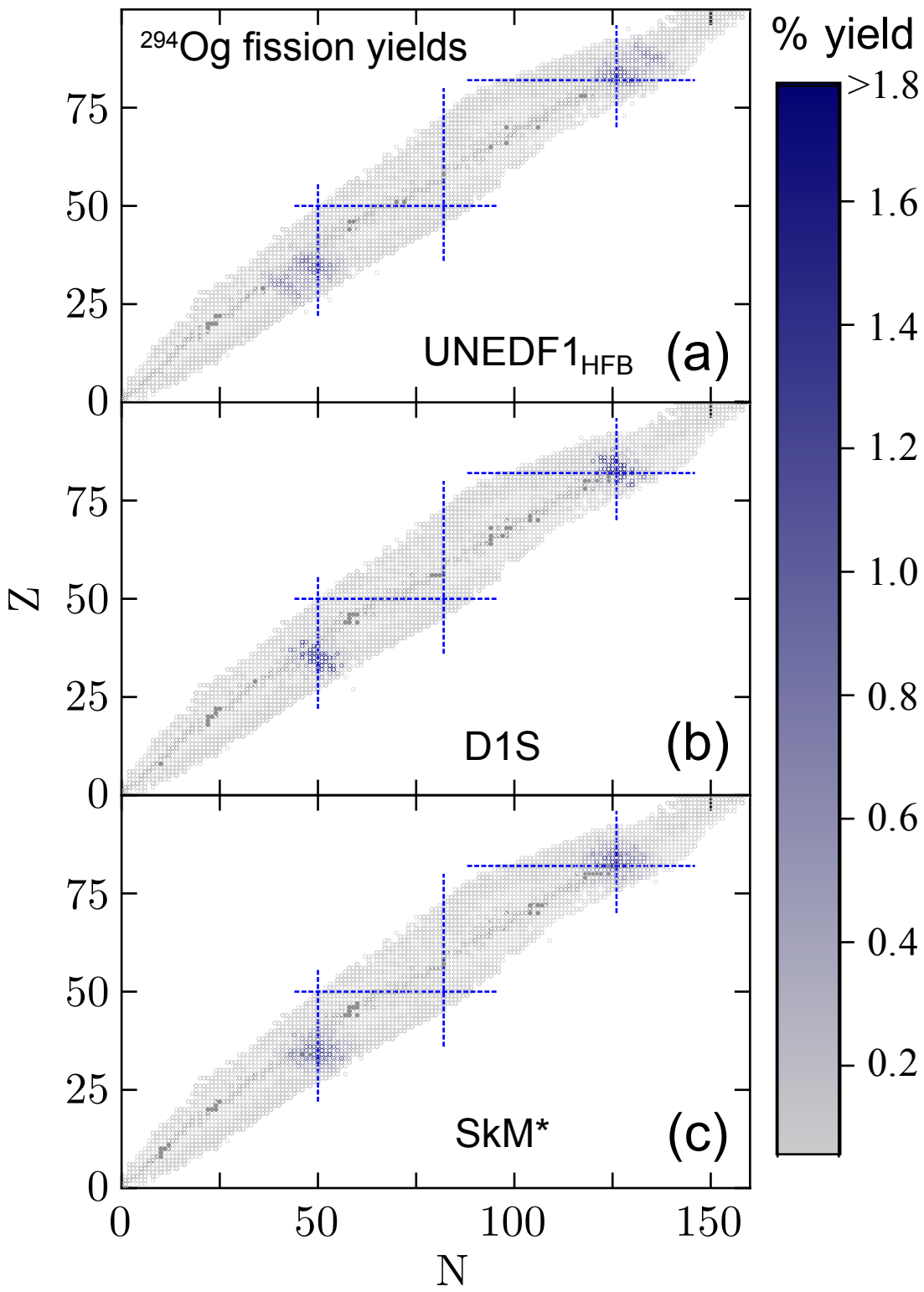

Figure 4.4: Fission fragment distributions for $^{294}_{118}\mathrm{Og}_{176}$ obtained in UNEDF1$_{\mathrm{HFB}}$ (a), D1S (b), and SkM* (c) EDFs using the non-perturbative cranking ATDHFB inertia and the baseline dissipation tensor η_0. Known isotopes are marked in grey [**?**]. Magic numbers 50, 82, and 126 are indicated by dotted lines.

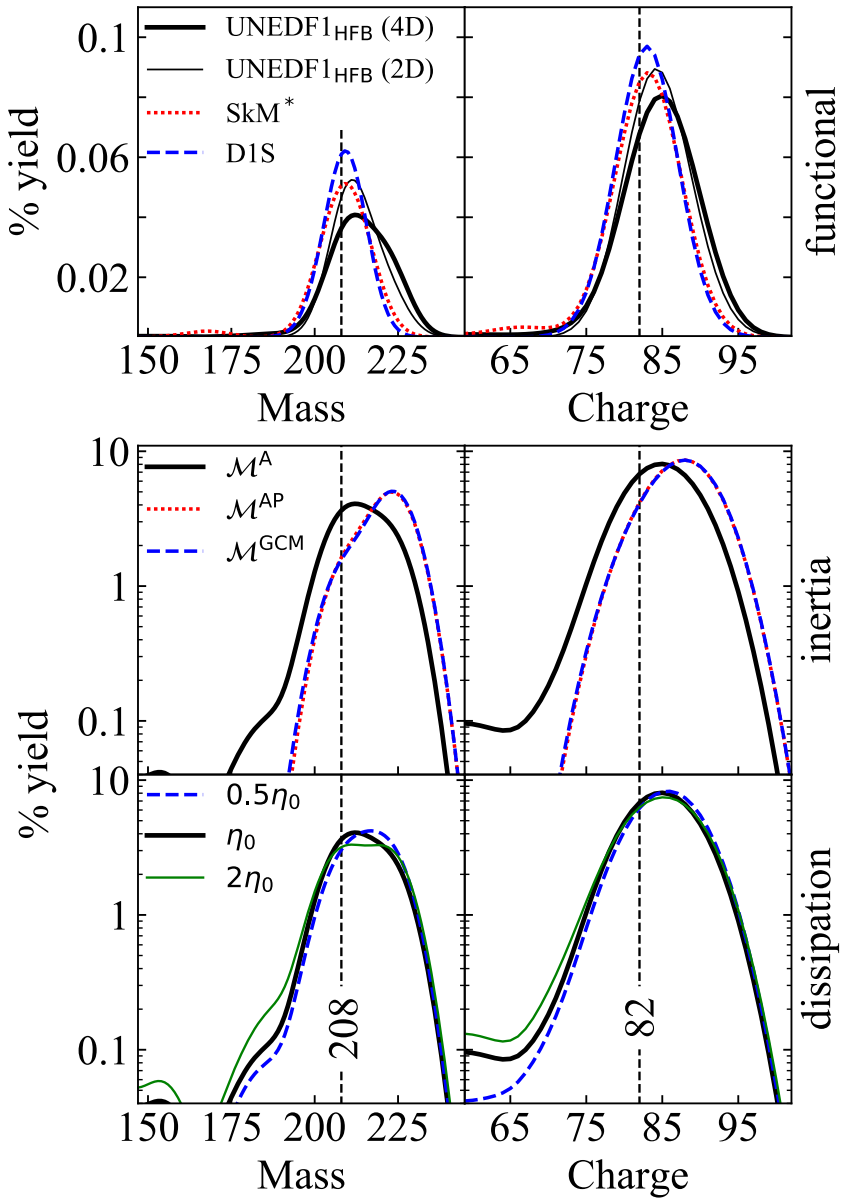

Figure 4.5: Upper panel: Predicted heavy fragment mass (left) and charge (right) yields of $^{294}_{118}\mathrm{Og}_{176}$ using different functionals (top, linear scale). Bottom panels: collective inertias and dissipation tensor strengths (in logarithmic scale). The baseline calculation was performed using the $\mathrm{UNEDF1_{HFB}}$ functional in a 4D space with non-perturbative cranking ATDHFB inertia and dissipation tensor strength η_0.

find that fluctuations do not affect the peak of the distribution, consistent with the results of Refs. [25, 65, 66]. The primary effect is in the tails.

4.3 Fragment formation in ^{294}Og

The Langevin dynamics approach is useful for calculating total yield distributions, but they do not offer much physical insight into the process of fragment formation. In order to better understand fragment formation for the most-probable fragments, we computed the nucleon localization function (section 2.1.4 and References [24, 25]) along the cluster emission path. This is shown in Figure 4.6, where it is compared to the fragments $^{208}_{82}\mathrm{Pb}_{126}$ and $^{86}_{36}\mathrm{Kr}_{50}$. We found that the lead prefragment is well-localized as early as just outside the outer turning line. The $N \approx 50$ neutrons belonging to krypton are also well-localized, but the $Z \approx 36$ protons are not, highlighting the importance of shell effects in prefragment formation.

In fact, we can leverage this insight to predict fission fragments as early as the outer turning line, resulting in a major reduction in total computing time because of the reduced PES. This is described in Chapter A.

4.4 Experimental efforts to find cluster emission in ^{294}Og

Perhaps the biggest uncertainty we'll see, or the biggest deviation from experiment, will be the distribution width. That's because we folded our Langevin results with a Gaussian function, the width of which was chosen rather arbitrarily to be $\sigma_A = 6, \sigma_Z = 4$. The values used in ^{240}Pu were 3 and 2, but the Q_N value they used to define scission was quite a bit smaller too. Since we had a much larger Q_N cutoff, we needed to account for larger particle number fluctuations. But these numbers were just kind of arbitrary. I'm not too worried

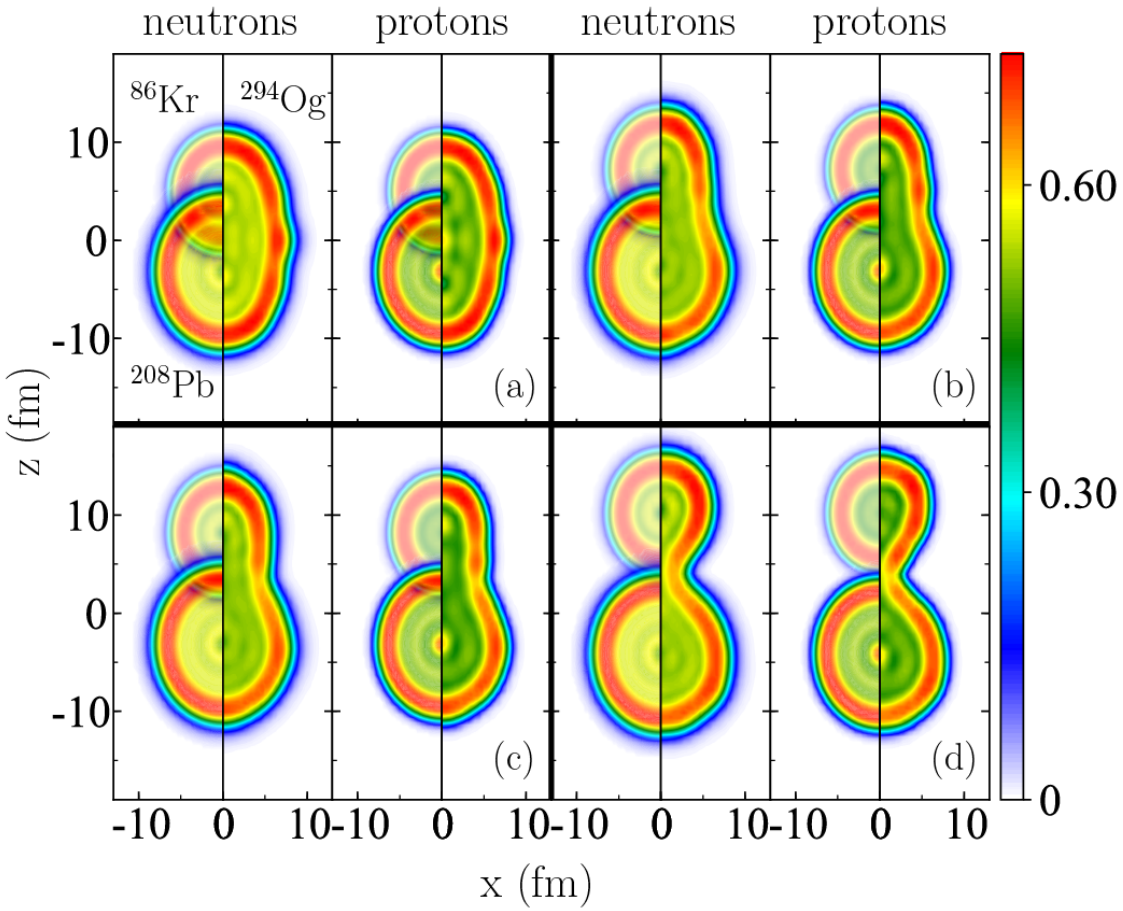

Figure 4.6: Nucleon localization functions for several deformed configurations of ${}^{294}_{118}\mathrm{Og}_{176}$. For comparison, localizations are shown for the fragments ${}^{208}_{82}\mathrm{Pb}_{126}$ and ${}^{86}_{36}\mathrm{Kr}_{50}$ on the left side of each subplot. The configurations shown correspond to Fig. 1 from the paper, with multipole moments (Q_{20}, Q_{30}) = (a) (75 b, 0); (b) (120 b, 17 $\mathrm{b}^{\frac{3}{2}}$); (c) (140 b, 24 $\mathrm{b}^{\frac{3}{2}}$); and (d) (264 b, 60 $\mathrm{b}^{\frac{3}{2}}$).

about this because the peak is the part that matters, and we clearly saw a peak at the cluster location.

The effort to detect cluster emission in superheavy elements is already underway. However, one of the biggest challenges standing in the way of observation of cluster emission from $^{294}_{118}\mathrm{Og}_{176}$ is the problem of statistics. There have only been 5 recorded instances of $^{294}_{118}\mathrm{Og}_{176}$, from the first observations in 2005 [67] to the most recent in [61].[1] To maximize the possibility of detecting SF events as they happen, there is some discussion in the experimental community about building an ionization chamber with the ability to distinguish fragments by their Z-value. This is discussed at some length in [61]:

"Among these SF events, there were signals correlated with incoming recoil-like signals within the time range of the 294Og half-life. We have inspected the possible assignment of some SF events to the fission of 294 Og. In the past, as well very recently, 294 Og was considered as a system consisting of doubly magic 208 Pb and singly magic N = 50, 86 Kr. These two components are well bound stable nuclei. One can envision that an asymmetric fission of 294 Og into 208 Pb and 86 Kr fragments might be somewhat enhanced.

"However, especially since the decay time of 294 Og is not sufficiently different from 258 No decay, one cannot make an assignment to 294 Og activity based only on the half-life of SF events. The energy of SF events vary, since we detect sometimes only a partial energy of fission fragments. Such events are more likely to arise from the SF activity produced in a multinucleon transfer involving the Cf isotope in the target. The indistinguishability of complete-fusion from transfer reaction products provides motivation for an ionization chamber, which would have a discrimination capability for the atomic number Z, placed before

[1] In fact, there were reports as early as 2004 [68] that there may have been detected instances of fission fragments resulting from the spontaneous fission of $^{294}_{118}\mathrm{Og}_{176}$, but these are unconfirmed.

the implantation Si counter. Construction and anticipated performance of such an ionization chamber based on gas electron multiplier (GEM) technology was recently discussed..."

Chapter 5

Fission in the r-process

5.1 The role of fission in the astrophysical r-process

One of the outstanding mysteries in astrophysics is the origin of heavy elements. It is thought that heavy elements are formed in a violent, neutron-heavy astrophysical scenario, such as a supernova or a neutron star merger, as light "seed" nuclei are rapidly bombarded by neutrons. This rapid neutron capture process, generally shortened to "r-process," increases the mass of seed nuclei until eventually they beta decay toward the valley of stability. This process is illustrated schematically in Figure 5.1.

Fission plays an important role in the r-process. The competition between neutron capture rates, fission rates, and other decays determines the direction in which the r-process proceeds. Fission also places an upper limit on the mass that can be produced in an r-process scenario, as fission lifetimes for heavy and superheavy isotopes become small enough to compete with the neutron flux of the environment around $N \approx 184$. Also, as will be discussed shortly, fissioning isotopes in this mass region are thought to lead to the rare earth peak around $A \approx 165$.

A related topic is the question of fission cycling. Once a heavy nucleus fissions, its fragments can then absorb more neutrons and make their way back up the r-process chain. Elemental abundance patterns in stars outside our solar system somewhat resemble that of

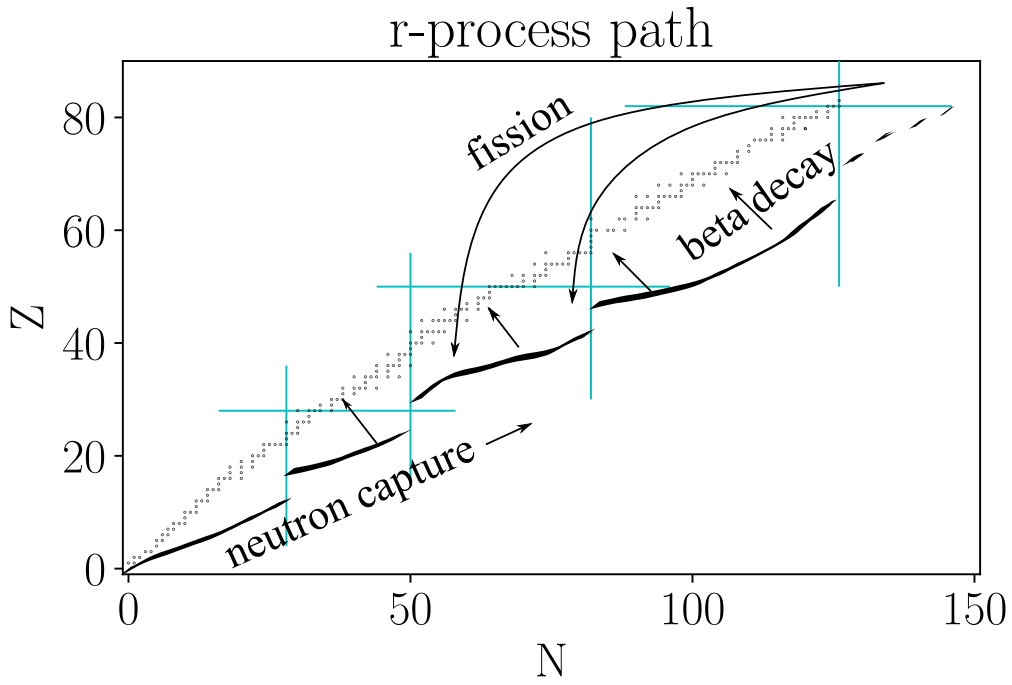

Figure 5.1: Schematic overview of the r-process. Neutron capture increases the mass of seed nuclei until they reach the drip line or decay, e.g. via beta decay or fission (spontaneous, beta-delayed, or neutron-induced).

our own [**?**], and it has been suggested that fission cycling may be responsible for this "universality" of the r-process [72].

R-process network calculations combine nuclear physics inputs, such as decay lifetimes, capture cross sections, and fission fragment yields, with astrophysical inputs, such as temperature and neutron flux, to simulate the complex competition between neutron capture and various forms of nuclear decay. Such calculations require quality inputs from a variety of sources. In order to guide experimental and theoretical efforts and to reduce uncertainties in the abundance pattern, sensitivity studies (in which inputs are tweaked to measure their impact on the final yield) can estimate the impact of a particular set of observables, such as fission fragment yields, on the r-process abundance pattern.

Sensitivity studies indicate that fission yields primarily affect the abundance and location of the rare earth peak and the second r-process peak ($A \approx 100 - 160$) [69, 70]. This can

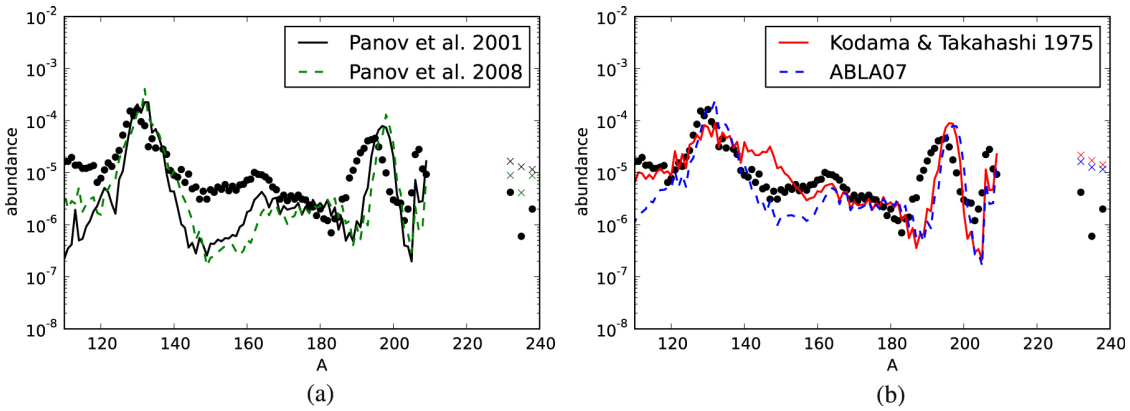

Figure 5.2: Quoting their caption: "Final abundances of the integrated ejecta around the second and third peak for an NSM (Korobkin et al. 2012; Rosswog et al. 2013) at a simulation time $t = 10^6$ s, employing the FRDM mass model combined with four different fission fragment distribution models (see the text). For reasons of clarity the results are presented in two graphs. The abundances for Th and U are indicated by crosses. In the left-hand panel the lower crosses belong to the Panov et al. (2008) model (dashed line), while the lower crosses in the right-hand panel belong to the ABLA07 distribution model (dashed line). The dots represent the solar r-process abundance pattern (Sneden et al. 2008)." [70]

be seen in Figure 5.2, in which four different sets of fission fragment yields were used to compute abundances. That this region should be sensitive to fission yields should come as no great surprise, since most fission fragments are likely to lie in the range $A \approx 100 - 160$.

In [73], the authors performed a sensitivity study in which, instead of assessing uncertainties, their goal was to isolate "hot spots" of nuclei that would have the greatest impact on the final r-process abundances. Four different mass models were used to estimate these hot spots; in Figure 5.3 the neutron-induced fission hot spots are shown, with the four different results superimposed on top of one another. We selected a few of these "hot spot" nuclei to analyze microscopically.

Figure 5.3 shows specifically neutron-induced fission; however, the phenomenological (GEF) yields that were used do not show a strong dependence on excitation energy for many nuclei of interest. Therefore, for simplicity, we simply calculate the spontaneous fission yields. A proper treatment of neutron-induced fission using a finite temperature

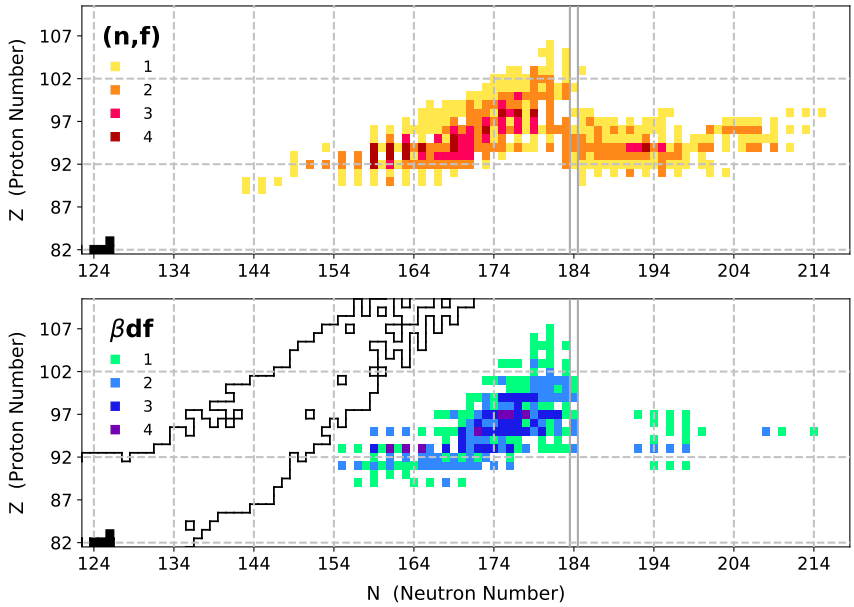

Figure 5.3: Heatmap showing isotopes whose fission yields are especially relevant to the r-process. This combines the results from four different mass models, and counts how many mass models found each isotope to be relevant (integrated fission flow above a certain threshold). [73]

formalism is being developed [42, 74, 75], but many challenges still remain (see Appendix, `\cite{cnr2018-proceedings}`).

5.2 Fission fragment yields for r-process nuclei

Using 5.3 as a guide, the isotopes ^{254}Pu, ^{264}Pu, ^{288}Pu, ^{270}Cm, and ^{276}Cf were selected for study. For each isotope, a 1D PES was calculated up to the outermost isomer state by constraining Q_{20} and leaving the other degrees of freedom unconstrained. Between the isomer state and the outer turning line, the PES was expanded to include Q_{30} in order to account for mass asymmetry between the fragments. The WKB method was used to estimate relative probabilities along the outer turning line, at which stage fragment pairs were identified using the localization-based method described in `\cite{locali, appendix}`.

The resulting distributions will be shown in Figure \ref{???} whenever I have them.

[Maybe the methods portion of this project, and/or the justification of the method, should be moved to another Appendix instead of the main body of the text. It's important, certainly, but it's not central to the narrative]

5.3 Kilonova and ^{254}Cf

An open questions about the r-process is where exactly it takes place. Core-collapse supernovae were a leading contender for years, but that hypothesis has recently fallen out of favor because of reasons \cite{???}. Bolstered by theoretical calculations \cite{???} and the neutron star merger event GW170817, neutron star mergers have become the site favored by many today. However, the results are far from conclusive, and stronger evidence is needed. The isotope $^{254}_{98}\mathrm{Cf}_{156}$ has been identified as a signature to help astronomers identify potential r-process sites.

It is suspected that the kilonova in a neutron star merger is produced by residual radioactivity as neutron-rich material produced in the merger decays toward stability. This material produces an observable light curve, which is one way to characterize the kilonova. The light curve will be dominated by alpha and beta decay events at early times, but if nuclei with spontaneous fission half-lives on the order of several days are produced in sufficient quantities, these would have a major impact on late-time heating in the kilonova, which in turn would affect the light curve. Thus, the shape of the light curve may indicate whether or not heavy, short-lived actinides were produced.

The question remains whether such nuclei exist which. Limiting ourselves to isotopes which have been experimentally measured, there are several which primarily undergo spon-

taneous fission and which may be produced in significant quantities in the r-process: several isotopes each of californium and fermium, plus ^{260}Md. However, most of the fermium and californium isotopes are too short-lived, and the population of ^{260}Md is highly model-dependent, leaving $^{254}_{98}\mathrm{Cf}_{156}$ as the most-likely candidate.

Perhaps you should cite [77], if no one else.

The effect of $^{254}_{98}\mathrm{Cf}_{156}$ on the heating and light curve depends on the energy released during fission, which in turn depends on the fragment yield it produces. Mass and kinetic energy distributions of $^{254}_{98}\mathrm{Cf}_{156}$ were actually measured in [78]. For some reason, though, Zhu considers that measurement "sparse" and they do some dressing up of it in their paper [77]. We decide to compute it microscopically using our Langevin approach, just to see what useful information we can add.

Chapter 6

Outlook

6.1 Review, outlook, and perspectives

In this chapter, it would be great to talk to everyone you know (Witek, Samuel, Jhilam, Nicolas, Michal, and so on) to get a better feel for what kinds of issues need to be addressed next. You've already got sort of a rudimentary understanding (see your Google Keep note for starters), but it might be good to get some outsider perspective. This will be especially important as you start looking for postdocs, and *especially* especially if you end up looking for postdocs in nuclear theory, but not necessarily nuclear fission.

As I said in chapter 1, "Finally, in chapter 6 we discuss the current state of the field, and, based on our experience, offer insights for guiding future developments in the field."

At this stage, we have techniques to calculate half-lives and primary fragment distributions (I haven't mentioned it yet, but there is also Nicolas' method for the fragment yields that uses TD-GCM. Are there others? What about for half-lives?). Some methods (such as Walid's, TDDFT, and possibly also this GCM method) are starting to estimate fragment energetics (kinetic and excitation energies). Down the line, there are others who try to predict neutron multiplicities and goodness knows what else using Hauser-Feshbach models and such (FREYA and more). These regions are still disconnected. Of course, these methods still need major refinements in order to better reflect experimental data. Some ideas currently in

the pipeline for improving the models are:

- Improved EDFs (here you could mention the DME EDFs; unfortunately, introducing density-dependence has a bad effect but I forgot what it was)
- Improved inertia tensor (such as automatic differentiation)
- Better/more collective coordinates (Walid's D, ξ coordinates from [28]; continuity of the PES in ∞-dimensional space such like in David Regnier's talks and papers)
- Fragment identification (our localization paper, Marc Verriere's method; you might also mention that this is not an issue in TDDFT, but there you've only got one single fragment pair)
- Microscopic/self-consistent description for dissipation. This is the mechanism which exchanges between intrinsic and collective degrees of freedom, but we handle it in a very ad hoc way with parameters which are fitted instead of determined systematically through some theory. Solving this problem will probably help us with the energetics of fragments (TKE and E* at the same time!)
- Machine learning for r-process inputs (described in detail in **??**)

Furthermore, there are more experimental observables that we should try to predict (refer to Andreyev's review to see what other observables can currently be measured). These include energetics (TKE and E*, for we have only begun to scratch the surface here), angular momentum, prompt neutron multiplicities (is that within the scope of these self-consistent models?), prompt neutron and gamma energy spectra spectra (getting harder; these are usually handled via statistical models; see intro to [33] for some references), level densities?,

and probably more but my mind is blanking. How to compute these in a self-consistent framework is still an open question. See also the outlook in Nicolas' review.

We definitely need a better handle on the inertia. The perturbative inertia is easy to compute, but not terribly reliable. The non-perturbative inertia can certainly do better, but as it is computed now (using finite differences) it is subject to numerical artifacts and instabilities (dependent on the level of convergence of the individual densities, the coefficient multipliers, different basis sizes) and actual physics, such as level crossings which manifest in projections from a higher-dimensional space.

UNEDF1 seems to underestimate fission barrier heights (artificial though the concept may be; the main impact is probably that lifetimes are underestimated). It also turns out to be a headache to work with, making convergence quite a challenge sometimes (any cases in particular, like for highly-deformed or heavy or octupole-deformed nuclei or something?). Better functionals might hope to better capture the physics, and one can hope they are easier to work with.

APPENDICES

Appendix A

Fragment Identification

A.1 Fragments and the Nucleon Localization Function

An improved scission criterion would go beyond simply counting the number of particles in the neck. To help with this, we have a tool at our disposal which helps us to understand correlations that affect fission dynamics. This is called the nucleon localization function, and it allows us to visualize the prefragment nuclear shell structure which largely determines the identity of fission fragments [24].

The nucleon localization function shows that some prefragments can be very well-formed even when the neck is large, while in another case the neck might be small but the prefragments, poorly-defined [25]. A better scission criterion should take into account, or at least be compatible with, the insights gained from the nucleon localization function. As noted in [79], fragment properties on either side of the scission line may differ drastically. This is because shell structure is not well-described geometrically. Our localization measure offers an alternative scheme for identifying fragments before the scission line (see [25]). Since it is based on the underlying quantum shells, it is less sensitive to fluctuations and particle rearrangements late in the evolution.

A.2 The problem of scission

For practical reasons we are limited to describing complicated shapes in terms of just a few parameters, leading to uncertainty in the fragment properties. In particular, the part of the process at which the neck snaps and one nucleus becomes two, called scission, is not well-defined in static approaches.

Many times in static approaches, including the results shown in this dissertation so far, scission is frequently characterized by a single number such as Q_N, which approximately corresponds to the number of particles in the neck. When that number falls below a certain predefined threshold, we say that the nucleus has scissioned. Fragments are identified and one can try to estimate the strength of the repulsive interaction forcing the fragments apart. Of course, as discussed by Younes and Gogny in [80**?**], wavefunctions corresponding to individual nucleons may extend into the spatial region of the opposite fragment.

This can be understood with an analogy: suppose we stretch a nucleus until a neck forms, and then we use a butcher knife to lop the two fragments apart. This works reasonably well for estimating fragment mass and charge, but it is very poor when it comes to estimating the relative energy of the fragments. To estimate fragment kinetic and excitation energies, one needs to carefully and delicately peel the interlocking fragments apart with a scalpel, or a proper accounting of entanglement and other many-body correlations.

Essentially what we show is that Q_N is meaningless, and that any static definition of scission is going to need to account for the actual configuration of the system.

A.3 Prefragment shell structure

A common theme in all of this has been the importance of the underlying shell structure of the prefragments. Shell energy corrections were found to be important in ${}^{178}_{78}\mathrm{Pt}_{100}$ and ${}^{180}_{80}\mathrm{Hg}_{100}$; cluster formation in ${}^{294}_{118}\mathrm{Og}_{176}$ was clearly influenced by the shell structure of the fragments; and the same may or may not be the case for ${}^{254}_{98}\mathrm{Cf}_{156}$. Let's discuss this.

We used localizations to visualize the internal/intrinsic shell structure inside nuclei, and we were able to see that this structure was sometimes intact early in the evolution, at times as far back as the outer turning line. And actually, this kind of makes sense. From just energetics alone, a nucleus on the outer turning line is just as happy (or just as stable, or just as settled) as a nucleus in the ground state. In some sense, it is formed. The difference now is just that the configuration it's in is now unstable due to Coulomb. The two halves, which are kind of maybe happy from a nuclear physics perspective, are pushing apart from the Coulomb repulsion. So that still has to be carried out, but the bulk of the physics might already be done at this point - though not necessarily. It *could* be that the fragments are well-formed and just pushing apart, but that may not be the case. It's like a divorce: sometimes the two have drifted so far apart, or are so well-defined and incompatible as individuals that the divorce is simple and relatively straightforward. Other times, it is a mess trying to sort out who gets what, and the two parties are fundamentally-changed by the proceedings.

I don't have any strong objections to Scamps and Simenel's octupole paper. In fact, to me it kind of makes sense: we've been saying, after all, that it's the shell structure of the deformed prefragments which determine scission, and not necessarily the final fragments themselves. That's really the whole idea behind the localization paper: we're seeing that, at least in some cases, the shell structure is pretty well intact early in the evolution, and that

those prefragments drive the system to scission with some shuffling of the neck nucleons at scission. All they're saying is that those neck nucleons will affect the shell structure of the prefragments, and just based on the kinds of shapes that the system will take (small neck connecting two elongated or spherical fragments), the prefragments have a strong octupole moment (regardless of whether the fragments are elongated or spherical). So it shouldn't be the spherical magic numbers we worry about, but the deformed (in this case, octupole-deformed) magic numbers.

I feel like it shouldn't be too terrible to investigate this claim. What if we constrained the multipole moment(s) that correspond(s) to octupole-deformed fragments (perhaps Q_{50})? I think this parameter might be included in Peter Moller's model, but not in ours.

A.4 Isospin transport

We're assuming that the parent nucleus gets to however it gets at the OTL (maybe it just happens to oscillate into that configuration randomly one day, and it feels reasonably stable there (per Witek's deformed harmonic oscillator paper)), and now we're trying to argue about how the neck nucleons will flow to rearrange themselves. So we're already imposing the assumption that the nucleons *will* flow from the neck to the fragments (and indeed, that at least seems to be what happens based on the success of this type of model so far).

This is indeed in contradiction with Scamps and Simenel's paper, because they essentially claim that once you get to that OTL configuration, the octupole deformation of the fragments (created by a spherical-ish prefragment with neck nucleons on the side, giving it a non-zero Q30) is sufficiently strong to snap the neck and let the fragments go on their merry way, octupole-deformed and everything. On the other hand, we're saying that instead, it's

just a lucky coincidence that the fragments are stable in an octupole-deformed configuration because they're not going to stay that way once the neck nucleons flow to their final destination.

There are these isospin transport papers essentially describe the flow of isospin and density in terms of the chemical potential and gradients. Nucleons will flow based on the chemical potential properties of the system, or in other words, to minimize the binding energy of the system. In general, that means you'll see a flow of neck nucleons in such a way as to bring the final fragments as [jointly] close to stability as possible.

The density gradient terms will lead to a flow of nucleons from prefragments to neck (with apparently a greater effect on neutrons than on protons).

Appendix B

Temperature-Dependent ATDHFB Collective Inertia

B.1

Everything which was shown in this dissertation assumed that the system was maintained at temperature $T = 0$ and the nucleus behaved as a superfluid below the Fermi surface. However, in many environments (such as a neutron star merger or a nuclear blast) there may be quite a bit of excitation energy imparted to the system, which would raise the temperature above the Fermi surface. In this case, pairs may be broken and the topology of the potential energy surface may change (see, for instance, [42]). In this case, the collective inertia of the system is changed, too, as shown below.

BIBLIOGRAPHY

[1] O. Hahn and F. Strassmann, Naturwissenschaften **27**, 11 (1939).

[2] L. Meitner and O. R. Frisch, Nature **143**, 239 (1939).

[3] G. Flerov and K. Petrjak, Phys. Rev. **58**, 89 (1940).

[4] N. Schunck and L. M. Robledo, Reports Prog. Phys. **79**, 116301 (2016).

[5] C. F. v. Weizs\"acker, Zeitschrift f\"ur Phys. **96**, 431 (1935).

[6] N. Bohr and J. A. Wheeler, Phys. Rev. **56**, 426 (1939).

[7] V. Strutinsky, Nucl. Phys. A **95**, 420 (1967).

[8] V. Strutinsky, Nucl. Phys. A **122**, 1 (1968).

[9] M. Brack, J. Damgaard, A. S. Jensen, H. C. Pauli, V. M. Strutinsky, and C. Y. Wong, Rev. Mod. Phys. **44**, 320 (1972).

[10] T. Baumann, M. Hausmann, B. Sherrill, and O. Tarasov, Nucl. Instruments Methods Phys. Res. Sect. B Beam Interact. with Mater. Atoms **376**, 33 (2016).

[11] G. Scamps and C. Simenel, (2018), arXiv:1804.03337 .

[12] G. Scamps, C. Simenel, and D. Lacroix, AIP Conf. Proc. **1681**, 040003 (2015).

[13] C. Simenel and A. S. Umar, Phys. Rev. C **89**, 031601 (2014).

[14] J. Grineviciute, P. Magierski, A. Bulgac, S. Jin, and I. Stetcu, Acta Phys. Pol. B **49**, 591 (2018).

[15] A. S. Umar, V. E. Oberacker, J. A. Maruhn, and P.-G. Reinhard, J. Phys. G Nucl. Part. Phys. **37**, 064037 (2010).

[16] G. Scamps, C. Simenel, and D. Lacroix, Phys. Rev. C **92**, 011602 (2015).

[17] A. Bulgac, S. Jin, K. Roche, N. Schunck, and I. Stetcu, (2018), arXiv:1806.00694 .

[18] R. Navarro Pérez, N. Schunck, A. Dyhdalo, R. J. Furnstahl, and S. K. Bogner, Phys. Rev. C **97**, 054304 (2018), arXiv:1801.08615 .

[19] M. Bender, P.-H. Heenen, and P.-G. Reinhard, Rev. Mod. Phys. **75**, 121 (2003), arXiv:9910025 [nucl-th] .

[20] J. Bartel, P. Quentin, M. Brack, C. Guet, and H.-B. Håkansson, Nucl. Phys. A **386**, 79 (1982).

[21] M. Kortelainen, J. McDonnell, W. Nazarewicz, P.-G. Reinhard, J. Sarich, N. Schunck, M. V. Stoitsov, and S. M. Wild, Phys. Rev. C **85**, 024304 (2012), arXiv:arXiv:1111.4344v2 .

[22] N. Schunck, J. D. McDonnell, J. Sarich, S. M. Wild, and D. Higdon, J. Phys. G Nucl. Part. Phys. **42**, 034024 (2015).

[23] P. Ring and P. Schuck, *The Nuclear Many-Body Problem*, edited by W. Beiglbock, M. Goldhaber, E. H. Lieb, and W. Thirring (Springer-Verlag, New York, 1980) p. 716.

[24] C. L. Zhang, B. Schuetrumpf, and W. Nazarewicz, Phys. Rev. C **94**, 064323 (2016), arXiv:arXiv:1607.00422v3 .

[25] J. Sadhukhan, C. Zhang, W. Nazarewicz, and N. Schunck, Phys. Rev. C **96**, 061301 (2017), arXiv:1711.10681 .

[26] J. Sadhukhan, W. Nazarewicz, and N. Schunck, Phys. Rev. C **93**, 011304 (2016), arXiv:1510.08003 .

[27] J. Sadhukhan, K. Mazurek, A. Baran, J. Dobaczewski, W. Nazarewicz, and J. A. Sheikh, Phys. Rev. C **88**, 064314 (2013), arXiv:1310.2003 .

[28] W. Younes and D. Gogny, *Fragment Yields Calculated in a Time-Dependent Microscopic Theory of Fission*, Tech. Rep. (Lawrence Livermore National Laboratory (LLNL), Livermore, CA (United States), 2012).

[29] A. Baran, J. A. Sheikh, J. Dobaczewski, W. Nazarewicz, and A. Staszczak, Phys. Rev. C **84**, 054321 (2011), arXiv:1007.3763 .

[30] S. A. Giuliani and L. M. Robledo, Phys. Lett. B **787**, 134 (2018).

[31] A. Baran, K. Pomorski, A. Lukasiak, and A. Sobiczewski, Nucl. Phys. A **361**, 83 (1981).

[32] A. Baran, Phys. Lett. B **76**, 8 (1978).

[33] K.-H. Schmidt and B. Jurado, Reports Prog. Phys. **81**, 106301 (2018), arXiv:1804.10421 .

[34] A. N. Andreyev, J. Elseviers, M. Huyse, P. Van Duppen, S. Antalic, A. Barzakh, N. Bree, T. E. Cocolios, V. F. Comas, J. Diriken, D. Fedorov, V. Fedosseev, S. Franchoo, J. A. Heredia, O. Ivanov, U. Köster, B. A. Marsh, K. Nishio, R. D. Page, N. Patronis, M. Seliverstov, I. Tsekhanovich, P. Van den Bergh, J. Van De Walle, M. Venhart, S. Vermote, M. Veselsky, C. Wagemans, T. Ichikawa, A. Iwamoto, P. Möller, and A. J. Sierk, Phys. Rev. Lett. **105**, 252502 (2010).

[35] V. Liberati, A. N. Andreyev, S. Antalic, A. Barzakh, T. E. Cocolios, J. Elseviers, D. Fedorov, V. N. Fedoseeev, M. Huyse, D. T. Joss, Z. Kalaninová, U. Köster, J. F. W. Lane, B. Marsh, D. Mengoni, P. Molkanov, K. Nishio, R. D. Page, N. Patronis, D. Pauwels, D. Radulov, M. Seliverstov, M. Sjödin, I. Tsekhanovich, P. Van den Bergh, P. Van Duppen, M. Venhart, and M. Veselský, Phys. Rev. C **88**, 044322 (2013).

[36] A. N. Andreyev, M. Huyse, and P. Van Duppen, Rev. Mod. Phys. **85**, 1541 (2013).

[37] J.-F. Martin, J. Taieb, A. Chatillon, G. Bélier, G. Boutoux, A. Ebran, T. Gorbinet, L. Grente, B. Laurent, E. Pellereau, H. Alvarez-Pol, L. Audouin, T. Aumann, Y. Ayyad, J. Benlliure, E. Casarejos, D. Cortina Gil, M. Caamaño, F. Farget, B. Fernández Domínguez, A. Heinz, B. Jurado, A. Kelić-Heil, N. Kurz, C. Nociforo, C. Paradela, S. Pietri, D. Ramos, J.-L. Rodríguez-Sànchez, C. Rodríguez-Tajes, D. Rossi, K.-H. Schmidt, H. Simon, L. Tassan-Got, J. Vargas, B. Voss, and H. Weick, Eur. Phys. J. A **51**, 174 (2015).

[38] A. N. Andreyev, K. Nishio, and K.-H. Schmidt, Reports Prog. Phys. **81**, 016301 (2018).

[39] J. Berger, M. Girod, and D. Gogny, Nucl. Phys. A **502**, 85 (1989).

[40] P. Möller, J. Randrup, and A. J. Sierk, Phys. Rev. C **85**, 024306 (2012).

[41] M. Warda, A. Staszczak, and W. Nazarewicz, Phys. Rev. C **86**, 024601 (2012), arXiv:arXiv:1205.5797v2 .

[42] J. D. McDonnell, W. Nazarewicz, J. A. Sheikh, A. Staszczak, and M. Warda, Phys. Rev. C **90**, 021302 (2014), arXiv:arXiv:1406.6955v1 .

[43] A. V. Karpov, V. I. Zagrebaev, Y. M. Palenzuela, and W. Greiner, , 1.

[44] M. Warda and J. L. Egido, Phys. Rev. C **86**, 014322 (2012), arXiv:1204.5867 .

[45] A. Sandulescu, D. Poenaru, and W. Greiner, Sov. J. Part. Nucl. **11**, 528 (1980).

[46] D. Poenaru, W. Greiner, K. Depta, M. Ivascu, D. Mazilu, and A. Sandulescu, At. Data Nucl. Data Tables **34**, 423 (1986).

[47] G. Royer, R. K. Gupta, and V. Denisov, Nucl. Phys. A **632**, 275 (1998).

[48] D. N. Poenaru, R. A. Gherghescu, and W. Greiner, Phys. Rev. Lett. **107**, 062503 (2011).

[49] D. N. Poenaru, R. A. Gherghescu, and W. Greiner, Phys. Rev. C **85**, 034615 (2012).

[50] D. N. Poenaru, R. A. Gherghescu, and W. Greiner, J. Phys. Conf. Ser. **436**, 012056 (2013).

[51] D. N. Poenaru, R. A. Gherghescu, W. Greiner, and N. S. Shakib, "How rare is cluster decay of superheavy nuclei?" in *Nucl. Phys. Present Futur.* (Springer International Publishing, Cham, 2015) pp. 131–140.

[52] D. N. Poenaru and R. A. Gherghescu, Phys. Rev. C **97**, 044621 (2018).

[53] K. P. Santhosh and C. Nithya, Phys. Rev. C **97**, 064616 (2018).

[54] Y. L. Zhang and Y. Z. Wang, Phys. Rev. C **97**, 014318 (2018).

[55] M. Warda and L. M. Robledo, Phys. Rev. C **84**, 044608 (2011), arXiv:1107.1478 .

[56] M. Warda, A. Zdeb, and L. M. Robledo, Phys. Rev. C **98**, 041602 (2018).

[57] D. N. Poenaru and W. Greiner, "Cluster radioactivity," in *Clust. Nucl. Vol. 1*, edited by C. Beck (Springer Berlin Heidelberg, Berlin, Heidelberg, 2010) pp. 1–56.

[58] H. J. Rose and G. A. Jones, Nature **307**, 245 (1984).

[59] A. Staszczak, A. Baran, and W. Nazarewicz, Phys. Rev. C **87**, 024320 (2013), arXiv:arXiv:1208.1215v1 .

[60] A. Baran, M. Kowal, P.-G. Reinhard, L. M. Robledo, A. Staszczak, and M. Warda, Nucl. Phys. A **944**, 442 (2015), arXiv:1503.01608 .

[61] N. T. Brewer, V. K. Utyonkov, K. P. Rykaczewski, Y. T. Oganessian, F. S. Abdullin, R. A. Boll, D. J. Dean, S. N. Dmitriev, J. G. Ezold, L. K. Felker, R. K. Grzywacz, M. G. Itkis, N. D. Kovrizhnykh, D. C. McInturff, K. Miernik, G. D. Owen, A. N. Polyakov, A. G. Popeko, J. B. Roberto, A. V. Sabel'nikov, R. N. Sagaidak, I. V. Shirokovsky, M. V. Shumeiko, N. J. Sims, E. H. Smith, V. G. Subbotin, A. M. Sukhov, A. I. Svirikhin, Y. S. Tsyganov, S. M. Van Cleve, A. A. Voinov, G. K. Vostokin, C. S. White, J. H. Hamilton, and M. A. Stoyer, Phys. Rev. C **98**, 024317 (2018).

[62] S. A. Giuliani, L. M. Robledo, and R. Rodríguez-Guzmán, Phys. Rev. C **90**, 054311 (2014).

[63] J. Sadhukhan, J. Dobaczewski, W. Nazarewicz, J. A. Sheikh, and A. Baran, Phys. Rev. C **90**, 061304 (2014), arXiv:arXiv:1410.1264v1 .

[64] P.-H. Heenen, J. Skalski, A. Staszczak, and D. Vretenar, Nucl. Phys. A **944**, 415 (2015).

[65] J. Randrup, P. Möller, and A. J. Sierk, Phys. Rev. C **84**, 034613 (2011).

[66] A. J. Sierk, Phys. Rev. C **96**, 034603 (2017), arXiv:1711.02234 .

[67] Y. T. Oganessian, V. K. Utyonkov, Y. V. Lobanov, F. S. Abdullin, A. N. Polyakov, R. N. Sagaidak, I. V. Shirokovsky, Y. S. Tsyganov, A. A. Voinov, G. G. Gulbekian, S. L. Bogomolov, B. N. Gikal, A. N. Mezentsev, S. Iliev, V. G. Subbotin, A. M. Sukhov, K. Subotic, V. I. Zagrebaev, G. K. Vostokin, M. G. Itkis, K. J. Moody, J. B. Patin, D. A. Shaughnessy, M. A. Stoyer, N. J. Stoyer, P. A. Wilk, J. M. Kenneally, J. H. Landrum, J. F. Wild, and R. W. Lougheed, Phys. Rev. C **74**, 044602 (2006).

[68] Y. Oganessian, V. Utyonkov, Y. Lobanov, F. Abdullin, A. Polyakov, I. Shirokovsky, Y. Tsyganov, G. Gulbekian, S. Bogomolov, B. Gikal, A. Mezentsev, S. Iliev, V. Subbotin, A. Sukhov, A. Voinov, G. Buklanov, K. Subotic, V. Zagrebaev, M. Itkis, J. Patin, K. Moody, J. Wild, M. Stoyer, N. Stoyer, D. Shaughnessy, J. Kenneally, and R. Lougheed, Nucl. Phys. A **734**, 109 (2004).

[69] S. Goriely, Eur. Phys. J. A **51**, 22 (2015).

[70] M. Eichler, A. Arcones, A. Kelic, O. Korobkin, K. Langanke, T. Marketin, G. Martinez-Pinedo, I. Panov, T. Rauscher, S. Rosswog, C. Winteler, N. T. Zinner, and F.-K. Thielemann, Astrophys. J. **808**, 30 (2015).

[71] J. d. J. Mendoza-Temis, M.-R. Wu, K. Langanke, G. Martínez-Pinedo, A. Bauswein, and H.-T. Janka, Phys. Rev. C **92**, 055805 (2015).

[72] J. Beun, G. C. McLaughlin, R. Surman, and W. R. Hix, Phys. Rev. C **77**, 035804 (2008).

[73] N. Vassh, R. Vogt, R. Surman, J. Randrup, T. M. Sprouse, M. R. Mumpower, P. Jaffke, D. Shaw, E. M. Holmbeck, Y.-L. Y. Zhu, Others, and G. C. Mclaughlin, , 1 (2018), arXiv:1810.08133 [nucl-th] .

[74] N. Schunck, D. Duke, H. Carr, and A. Knoll, Phys. Rev. C **90**, 054305 (2014), arXiv:1311.2616 .

[75] N. Schunck, D. Duke, and H. Carr, Phys. Rev. C **91**, 034327 (2015), arXiv:1311.2620 .

[76] S. Goriely, J.-L. Sida, J.-F. Lemaître, S. Panebianco, N. Dubray, S. Hilaire, A. Bauswein, and H.-T. Janka, Phys. Rev. Lett. **111**, 242502 (2013).

[77] Y. Zhu, R. T. Wollaeger, N. Vassh, R. Surman, T. M. Sprouse, M. R. Mumpower, P. Möller, G. C. McLaughlin, O. Korobkin, T. Kawano, P. J. Jaffke, E. M. Holmbeck, C. L. Fryer, W. P. Even, A. J. Couture, and J. Barnes, Astrophys. J. **863**, L23 (2018).

[78] R. Brandt, S. G. Thompson, R. C. Gatti, and L. Phillips, Phys. Rev. **131**, 2617 (1963).

[79] W. Younes and D. Gogny, Phys. Rev. C **80**, 054313 (2009), arXiv:0910.1284 .

[80] W. Younes and D. Gogny, Phys. Rev. Lett. **107**, 132501 (2011), arXiv:1103.3466 .